https://doi.org/10.5194/egusphere-2024-1385
Preprint. Discussion started: 12 July 2024

Measurement report: Sources and meteorology influencing highly-time resolved $PM_{2.5}$ trace elements at 3 urban sites in extremely polluted Indo Gangetic Plain in India.

Ashutosh K. Shukla[1], Sachchida N. Tripathi[1,2]*, Shamitaksha Talukdar[1], Vishnu Murari[1], Sreenivas Gaddamidi[1], Manousos-Ioannis Manousakas[3], Vipul Lalchandani[1], Kuldeep Dixit[4], Vinayak M. Ruge[5], Peeyush Khare[3], Mayank Kumar[6], Vikram Singh[7], Neeraj Rastogi[8], Suresh Tiwari[9], Atul K. Srivastava[9], Dilip Ganguly[10], Kaspar Rudolf Daellenbach[3], Andre. S. H. Prevot[3*]

[1]Department of Civil Engineering, Indian Institute of Technology Kanpur, Uttar Pradesh, 208016, India
[2]Department of Sustainable Energy Engineering, Indian Institute of Technology Kanpur, Uttar Pradesh, 208016, India
[3]Laboratory of Atmospheric Chemistry, Paul Scherrer Institute, Villigen PSI, 5232, Switzerland
[4]School of Public & International Affairs, Virginia Tech Blacksburg, Virginia, 24060, USA
[5]Tesscorn AeroFluid, Inc. 50, 3rd Floor, 100 Feet Road, Koramangala 2nd Block, Bangalore 560034, India
[6]Department of Mechanical Engineering, Indian Institute of Technology Delhi, New Delhi 110016, India
[7]Department of Chemical Engineering, Indian Institute of Technology Delhi, New Delhi -110016, India
[8]Geosciences Division, Physical Research Laboratory, Ahmedabad, 380009, India
[9]Indian Institute of Tropical Meteorology, Ministry of Earth Sciences, New Delhi, India
[10]Centre for Atmospheric Sciences, Indian Institute of Technology Delhi, New Delhi, 110016, India

*Correspondence to S. N. Tripathi (snt@iitk.ac.in) and André S. H. Prévôt (andre.prevot@psi.ch)

https://doi.org/10.5194/egusphere-2024-1385
Preprint. Discussion started: 12 July 2024

Abstract

High time-resolution aerosol measurements across various regions of the Indo-Gangetic Plain (IGP) are essential due to its dense population, intense industry, pollution episodes, agriculture, health impacts, and climate implications. However, absence of studies in Central IGP (C-IGP) limits the comprehensive understanding, as research has been primarily concentrated in Upper IGP (U-IGP) with limited spatial coverage. To address this gap, the study aimed to provide insights into elemental concentrations, sources, regional comparisons, seasonal variations, meteorological influences, and health risks using Xact at three urban sites in U-IGP and C-IGP regions. During cold, S, Cl, and K were major contributors to elemental-PM2.5, while warm periods exhibited significant variations in Al, Si, Sr, and Ba concentrations, indicating seasonal influences on pollution levels. Average concentrations of carcinogenic elements (Pb, Ni, As, and Cr) typically stayed below recommended levels, but individual exceedances of Pb was 40-50% during both periods in U-IGP, linked to coal combustion and lead smelting. Positive Matrix Factorization (PMF) using ME-2 (Multilinear Engine2) solver was performed, resolving Cl-rich, coal combustion, Cu-rich, dust, SFC1 (Solid fuel combustion 1), SFC2, and S-rich. Cl-rich, S-rich, and SFC1 in both regions, with differences observed in their relative contributions, indicating the influence of regional emissions. Role of meteorology in variation of elemental-PM2.5 during clean and polluted episodes in IGP regions were observed. During pollution episodes, when PM2.5 concentrations showed sharp increase as compared to clean periods especially during cold, the relative contribution of Cl-rich increased which is due to the condensation of Chloride during low temperature, indicating the role of steel industries as well as trash (plastic and PVC (Polyvinyl Chloride) mixed) in the pollution episode as well as haze formations. However, the clean periods during warm were dominated by Dust and S-rich. Overall, the study highlights the variation of elemental pollution across IGP regions, its health impact and factors driving the pollution episodes. These findings aid in understanding spatial and temporal dynamics of elemental pollution, informing mitigation strategies and policies for public health protection in the region.

https://doi.org/10.5194/egusphere-2024-1385
Preprint. Discussion started: 12 July 2024

Keywords:

Indo-Gangetic plain; Source Apportionment; trace elements; $PM_{2.5}$; health risk

1 Introduction

Air pollution is a major threat to global health, causing seven million deaths each year (Fuller et al., 2022). In India alone, 1.67 million deaths in 2019 were due to air pollution, accounting for 17.8% of total deaths, with most of these deaths caused by ambient particulate matter (PM) pollution (Pandey et al., 2021). Airborne heavy metals though a minor fraction of $PM_{2.5}$ but are of a particular concern due to their ability to be absorbed in the bloodstream and accumulate in vital organs (Kastury et al., 2017; Rehman et al., 2018; Giordano et al., 2013). Even brief exposure to these elemental species can cause health problems such as headaches, vomiting, and abdominal pains (Geiger et al., 2010; Kloog et al., 2013; Strickland et al., 2015; Huang et al., 2012). The impacts of trace element exposure can also be affected by dynamic weather conditions and type of emission sources (Tchounwou et al., 2012; Holden et al., 2016).

An alarming rise in atmospheric PM, especially in India's Indo-Gangetic Plain (IGP) due to urbanization, industrialization, and biomass burning, necessitates attention (Pant et al., 2015). During winter, IGP experiences significant PM2.5 increases, affecting a large population (Ojha et al., 2020; Majumdar et al., 2021). Climate variation between warm and cold periods influences pollution levels (Bhat et al., 2017; Kumar et al., 2020; Dumka et al., 2021). Recent studies highlight Indian cities, mostly in the IGP, among the world's top PM2.5 hotspots (IQAir, 2022). Favorable winter conditions transport pollutants eastward, impacting the subcontinent (Jat et al., 2021; Mahapatra et al., 2018). While upper-IGP (U-IGP) had more PM studies, particularly on particulate-bound organic aerosols, central-IGP (C-IGP) and lower-IGP (L-IGP) lack focus (Yadav et al., 2022). Source apportionment studies, mostly in Delhi, rely on offline filter analysis (Jain et al., 2017; Sharma et al., 2016; Nagar et al., 2017). Metal constituent studies at IIT Delhi reveal various sources, including road dust and waste burning (Das et al., 2020; Jain et al., 2020). PMF model analysis by Sharma and Mandal (2017) identifies major elemental sources such as secondary aerosols, soil dust, vehicle emissions, fossil fuel burning, biomass

https://doi.org/10.5194/egusphere-2024-1385
Preprint. Discussion started: 12 July 2024

burning, industrial emissions, and sea salts. Fewer studies in C-IGP indicate dominance of crustal elements and significant anthropogenic contributions (Pandey and Soni, 2017; Rai et al., 2016). Offline sampling limitations underscore the need for real-time monitoring to capture short-term pollution events (Cooper et al., 2010). Most offline filter-based source apportionment studies utilize statistical multivariate methods like receptor models, benefiting from inter-sample variability and real-time ambient elemental species monitoring essential for trace element source research and human health effects.

Recently, few SA studies on elemental data with high-time resolution had been performed in U-IGP (Delhi) only (Rai et al. 2020b; Shukla et al. 2021; Manchanda et al. 2022). Rai et al. (2020b) observed that during the warm period, crustal elements contributed more relative to the overall total than they did during the cold period, while the opposite was true for Cl. Another real-time elemental study by Shukla et al. (2021) identified 8 factors using elemental PMF, with dust being the most prominent (52.5%). Secondary oxidized sources were found to dominate during summer, accounting for 27% (excluding dust), highlighting the need for reducing the precursors of secondary aerosols in Delhi. A study by Manchanda et al. (2022) found an episodic fireworks factor attributed to Diwali which led to distinct peaks in K, Al, Sr, Ba, S, and Bi concentrations, which were identified as tracers. Further SA analysis found that fireworks accounted for 95% of elemental part of $PM_{2.5}$ (El-$PM_{2.5}$) during Diwali. The existing literature has primarily focused on U-IGP, particularly Delhi, and lacks comprehensive studies that include multiple sites in different parts of the IGP region.

In our study, we performed measurements at three distinct urban sites in the IGP region with two in U-IGP (Delhi-NCR) and other in C-IGP (Lucknow) to understand the variation of El-$PM_{2.5}$ in the IGP region. We have also performed the PMF using ME-2 for source apportionment of elements to further understand the spatial and temporal variation of elemental sources within the U-IGP (between 2 sites in Delhi viz. Indian Institute of Technology, Delhi (IITD) and Indian Institute of Tropical Meteorology, New Delhi branch (IITMD)) region and variation between U-IGP and C-IGP region. For investigation of the role of meteorology we have discussed the variation of sources between cold and warmer periods at these three sites. We had also compared the diurnal variation of sources during the warm and cold periods in the U-IGP and C-IGP regions to understand the dynamic behavior of sources. This study

https://doi.org/10.5194/egusphere-2024-1385
Preprint. Discussion started: 12 July 2024

further aims to identify and understand the key factors contributing to air pollution episodes characterized by high $PM_{2.5}$ mass loadings, specifically focusing on elemental sources and their relationship with specific meteorological conditions. The findings will contribute to a more comprehensive understanding of elemental pollution sources, their spatial and temporal variations, and their implications for human health in the IGP region. This research will provide valuable insights for developing targeted mitigation strategies and policies to combat air pollution and protect public health in this heavily affected region.

2 Material and Methods

2.1 Sampling details

The IGP is a densely populated region that spans over 255 million hectares of fertile land in northern and eastern India, Pakistan, and Bangladesh (Fig. S1). The IGP can be divided into three distinct regions based on geographical location: the U-IGP, C-IGP and L-IGP. The U-IGP region includes the Indus plain of Pakistan and Indian states of Punjab, Haryana, and Delhi and is characterized by high population density, industries, brick-kilns, biomass-based energy, traffic exhaust emissions and vast agricultural land. The C-IGP region covers the states of Uttar Pradesh, Bihar, and parts of Jharkhand, is influenced by both long and regional transport of mineral dust, power plant emissions, crustal re-suspensions, crop-residue burning, household cooking, industries, and vehicular emissions. The L-IGP region encompasses all of West Bengal and Bangladesh and is the final region in the IGP.

https://doi.org/10.5194/egusphere-2024-1385
Preprint. Discussion started: 12 July 2024

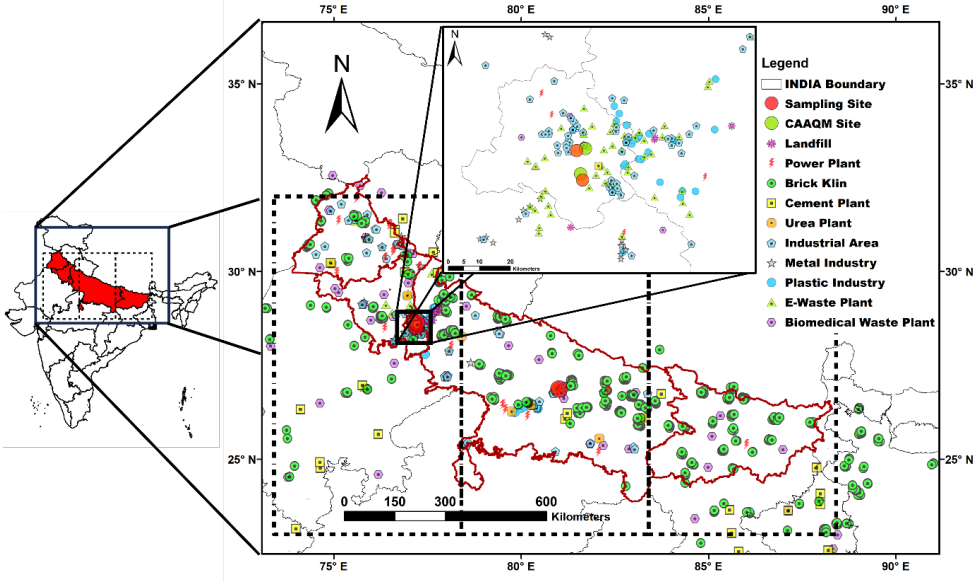

134 Figure 1. Detailed map with the sampling locations and the nearest government monitoring CAAQMS stations (shown in red circle) in the IGP region. The possible trace element sources have also been
136 shown in the map. The inset picture zooms the sampling sites and industrial emission sources in the U-IGP region.

138

140 In U-IGP, two sites were selected for sampling: Indian Institute of Technology Delhi, Hauz Khas (U-IGP1) (28.54°N, 77.19°E) and Indian Institute of Tropical Meteorology, New Delhi branch, Pusa Forest
142 (U-IGP2) (28.63°N, 77.17°E). The U-IGP2 is situated in the central region of Delhi and is surrounded by residential areas, educational and research institutions, a major traffic road, and the Pusa Hill Forest.
144 U-IGP1 is located inside the campus of an educational institution (IITD) in south Delhi and is also surrounded by residential and market areas, educational institutions, and a major traffic emissions
146 source (outer ring road). These sites represent the urban emissions in Delhi, which include power plants, medium and small-scale industries, brick kilns, vehicles, domestic cooking, and seasonal agricultural
148 waste burning from neighboring states of Punjab and Haryana.

The C-IGP1 sampling site is in Lucknow city, Uttar Pradesh, at Uttar Pradesh Pollution Control Board
150 (UPPCB) office building in Gomti Nagar (26.87°N, 81.00°E). The site has a diverse emissions as it is surrounded by residential buildings, hotels, low-income households, office complexes, railway station,

https://doi.org/10.5194/egusphere-2024-1385
Preprint. Discussion started: 12 July 2024

big commercial spaces, and a web of roads with a major highway nearby. The industrial and manufacturing plants in and around the city are involved in steel metal components and fabrication, metal industry, cement industry, chemical industries, urea plants, and biomedical waste plant. An industrial map (Fig.1) of IGP region shows major and mini-industrial areas, large and medium scale industries, sugar mills, pharmaceutical industries, and power plants.

Table 1. Summary of the meteorological parameters and sampling for the warm and cold periods at the three sites in the IGP region.

	U-IGP1		U-IGP2		C-IGP1	
(Mean±S.D)	Warm	Cold	Warm	Cold	Warm	Cold
Temp (°C)	23.3±5.2	12.9±4.9	21.2±6.1	12.5±5.3	25.6±6.7	15.4±5.2
R.H (%)	67.9±13	79.7±13.3	61.6±17.4	74.8±12.5	46.0±19.7	74.2±20.8
PBLH (m)	506.2±663.2	347.0±365.4	546.6±78	376.1±338.8	697.4±900.1	394.0±416.8
Solar radiation (W/m^2)	86.8±125.2	60.7±97.3	115±167	68±102	186±246.5	106±156.2
Sampling period	1st Oct- 26th Nov	27th Nov-08th Jan	1st Oct-26th Nov	27th Nov-08th Jan	25th Feb-30th Apr	15th Dec-25th Feb

To quantify the chemical composition of ambient PM with high temporal resolution, we deployed an combination of aerosol instruments with high-time resolution measurements at three distinct locations. Further to understand the role of meteorology and their effect to the elements and their sources, the sampling period was divided into cold and warm periods, the summary of the sampling and meteorology for the same is provided into the Table 1. Elemental species were monitored between October 1, 2019 and April 30, 2021 at all three sites. The U-IGP1 sampling site was located on the 3rd floor of the Centre for Atmospheric Science (CAS) building in IITD, where the Xact instrument was used to collect

https://doi.org/10.5194/egusphere-2024-1385
Preprint. Discussion started: 12 July 2024

aerosols via a $PM_{2.5}$ cutoff cyclone installed on the rooftop side. The sampling system was equipped with a heater to maintain a relative humidity at 45%, and a temperature-controlled laboratory ensured consistent measurement conditions. The U-IGP2 utilized a similar setup, with instruments located in a temperature-controlled laboratory on the second floor and sampling performed through a $PM_{2.5}$ cutoff cyclone connected to a long sampling tube. Sampling methods and measurement sites in U-IGP were described in detail in our companion papers, including Shukla et al., 2023; Lalchandani et al., 2022 and Manchanda et al., 2022. At the C-IGP1, the online instruments were housed in a temperature-controlled laboratory located ~12 m above the ground level in the Uttar Pradesh Pollution Control Board (UPPCB) office building in Gomti Nagar (Jain et al., 2023). The Xact instrument was similarly installed in a customized enclosure suitable for instrument operation (temperature variation from 20°C to 25°C) on the rooftop, with a heater used to maintain a relative humidity level around 45% during aerosol collection.

2.2 Instruments

The Xact ambient metal monitor provides a continuous, real-time concentration of elements in PM. The device and its use are described in detail in the literature (Thomas Kelly, Amy Dindal and Battelle John McKernan, 2012). In brief, ambient aerosol is sampled at 16.7 lpm rate and it deposits on the filter tape (deposit area 0.487 cm^2) and transported to the analysis area for energy dispersive X-ray fluorescence (EDXRF). In this method, three distinct energies conditions (EC) are used to irradiate the deposit area. Excited X-ray fluorescence is detected using a silicon drift detector (SDD). After determining which element contributed to the spectral peak intensity using the spectral deconvolution method, the elemental concentrations are acquired utilizing analysis software.

The elements Al, Si, S, Cl, K, Ca, Ti, Cr, Mn, Fe, Co, Ni, Cu, Zn, As, Se, Br, Rb, Sr, Zr, Mo, Cd, In, Sn, Sb, Te, Ba, Pb, Bi, and Bi were all measured using the Xact metal monitor at a half-hourly temporal resolution. The flow rate was calibrated with a standard flowmeter (Field flow calibrator, ALICAT scientific), and the instrument's setup was regulated with measurements of the surrounding temperature and pressure to provide quality assurance and quality control (QA/QC). At twelve o'clock (midnight), chromium, lead, and cadmium in a known sample were used to calibrate the spectrum by measuring

https://doi.org/10.5194/egusphere-2024-1385
Preprint. Discussion started: 12 July 2024

their intensities (00:15 to 00:30). During the energy alignment procedure, a Cr and Niobium (Nb) rod is used to place the spectral peaks for each element at the appropriate energy levels and thus calibrate the energy spectrum. Daily QA Upscale statistics for these metals were within 10%. Each sample of ambient air is compared to a known value from the instrument's internal Nb source. Leak and flow checks were done at the beginning and end of the campaign, and the XRF calibration check was performed using thin film standards of elements, yielding a result well below the 5% limit. Since the cyclone was subject to heavy loadings from the frequent pollution events, it was periodically cleaned.

At these three locations, non-refractory (NR) $PM_{2.5}$ concentrations were measured in real time using high-resolution time-of-flight aerosol mass spectrometers (Aerodyne Inc., USA). BC concentration was monitored in real time across all three locations using aethalometers (AE-33, Magee Scientific, Berkeley, CA, USA). We only use AMS and BC data to compare it to the factor time series of the elements, as it is the focus of other research studies.

Supplementary data of precipitation and PBLH (planetary boundary layer height) were extracted from the grid over Delhi and Lucknow for all three sites using the Meera-2 satellite while temperature (only at U-IGP1), relative humidity (RH at C-IGP1 only) also used from the satellite data (Gelaro et al., 2017). Wind speed (WS) and wind direction (WD) data for U-IGP1 were acquired using GFS model simulations with a horizontal resolution of 25x25 km. The CO and NOx data for U-IGP1 were measured using gas analyzers (ECOTECH Serinus 30 CO analyzer; ECOTECH Serinus 40 oxides of nitrogen analyzer). Data for O_3, SO_2, and SR (solar radiation) at U-IGP1 were acquired from the nearest Central Pollution Control Board (CPCB) air quality monitoring site at R.K. Puram (Fig.1). $PM_{2.5}$ concentrations are measured at the U-IGP1 using a beta-attenuation monitor (BAM). Other parameters such as CO, NOx, O_3, SO_2, Solar radiation (SR), WS, WD, and $PM_{2.5}$, Temperature were acquired from the nearest air quality monitoring site administered by CPCB (from Mandir Marg at U-IGP2) and UPPCB (at C-IGP1), respectively, for the U-IGP2 and C-IGP1.

2.3 Source apportionment (SA) using ME-2 solver

The PMF model is a powerful tool for SA of ambient aerosol measurements. It is a bilinear receptor model that enforces non-negative constraints and has been widely used in the scientific community

https://doi.org/10.5194/egusphere-2024-1385
Preprint. Discussion started: 12 July 2024

(Paatero & Tapper, 1994). Mathematically, PMF can be described by Equation (1), which represents a bilinear factor analysis model.

$$x_{ij} = \sum_{k=1}^{p} g_{ik} \cdot f_{kj} + e_{ij} \quad (1)$$

where the measured concentration of species (x_{ij}) is represented as the sum of the product of the source profile (f_{kj}) and its time series (g_{ik}), along with a residual matrix (e_{ij}). To minimize the objective function (Q) and solve for the bilinear Equation, PMF uses the least square technique. This objective function (Q), (Equation (2)), involves the squared ratio of residuals (e_{ij}) and the measured uncertainty (σ), summed across all samples.

$$Q = \sum_{i=1}^{m} \sum_{j=1}^{n} \left(\frac{e_{ij}}{u_{ij}}\right)^2 \quad (2)$$

where m and n represent the number of samples and variables (species), respectively. In the field of source apportionment of ambient measurements, PMF is a popular bilinear unmixing receptor model that does not require any prior information. However, the ME-2 implementation of PMF takes advantage of the a-value approach, which allows for more efficient exploration of the rotational space by enabling a priori information to be incorporated. This approach is advantageous as it allows for greater control of rotations and access to the full rotational space, as compared to PMF alone. By using scalar a-values ranging from 0 to 1, one or more factor profiles can be constrained, as outlined in Equation (3), Recent studies by Belis et al. (2019a) and Paatero and Hopke, (2009) have also demonstrated the effectiveness of the a-value approach in enhancing the accuracy and precision of source apportionment results.

$$f'_{kj} = f_{kj} \pm a \times f_{kj} \quad (3)$$

The bilinear unmixing receptor model ME-2 was applied to the ambient data, utilizing the Source Finder tool (SoFi Pro v 6.8, Datalystica Ltd, Villigen, Switzerland), which offers a user-friendly interface for implementing and investigating various rotational techniques with ease (Canonaco et al., 2020, 2013). The analysis was conducted using Igor Pro v6.37 software (Wavemetrics, Inc., Portland, OR, USA). This approach enabled the efficient and controlled exploration of the rotational space, allowing for a comprehensive and detailed examination of the data. By leveraging this approach, we were able to gain

https://doi.org/10.5194/egusphere-2024-1385
Preprint. Discussion started: 12 July 2024

a deeper understanding of the underlying sources and their respective contributions to the measured concentrations.

For the input data matrix preparation, the elements detected at half-hourly time resolution was filtered based on the percentage of data points below their Minimum Detection Limit (MDL) (supplied by manufacturer: Cooper Environmental Services). 19 elements were found to have 80% of their data points above MDL and were used in the PMF input (Si, S, Cl, K, Ca, Ti, V, Cr, Mn, Fe, Ni, Cu, Zn, As, Se, Br, Rb, Sr, and Pb at all three sites; additional 4 elements : Al, Zr, Sb, and Ba at U-IGP1; and additional 3 elements: Al, Sn, and Ba at U-IGP2). The spectrum deconvolution uncertainty and the measurement uncertainty were used to generate the error matrix, which was then obtained directly from the Xact software (Tremper et al., 2018). The input matrix for U-IGP1 consists of 4532 data points (same time resolution as raw data) and 23 elements (for U-IGP2, 4190 timestamps x 22 elements and for C-IGP1, 4047 timestamps x 19 elements). Variables with S/N ratios below 2 had their weights reduced by swapping out their individual values with the appropriate 2/SNR value. It has been shown that data periods with high SNR in a variable are unaffected by down weighting the value of individual cells (Rai et al., 2020).

The unconstrained PMF was executed from 3 to 11 factors, and it was applied to the elemental dataset. In brief, first point of investigation of the optimum number of factor solution was to observe the change in Q/Qexp (7-factor solution at all the three sites). Further the final environmentally feasible solution was selected by observing the criterion of physical meaningful factors, time series, diurnal variation, scaled residual, Q_residual, unexplained variation and correlation with external tracers. Complete discussions of both optimum factor selection and describing the final ME-2 results can be found in the supplementary sections S1 and S2, respectively.

2.4 Uncertainty estimate of elemental ME-2 SA results

To capture the statistical dependence on random changes in the data, the bootstrapping analysis creates numerous bootstrap distributions with the exact dimensions as the original dataset, then computes the necessary statistics from each bootstrap distribution (Brown et al., 2015; Stefenelli et al., 2019). Random values of the constrained information were also employed, in addition to the random

https://doi.org/10.5194/egusphere-2024-1385
Preprint. Discussion started: 12 July 2024

resampling of the PMF input (bootstrap), and the random a-value seeks to accurately quantify the rotational uncertainty of the solution (Tobler et al., 2020). To evaluate statistical and rotational uncertainty, the input data matrix was repeatedly (n=500) and randomly resampled (bootstrap approach), with a random a-value for the constrained variables selected each time. A set of criteria (R-Pearson correlation between base factor time series and BS recovered factor time series) was utilized to select environmentally meaningful and stable solutions because there were so many PMF runs to investigate manually. According to Canonaco et al. (2020), the time series for each bootstrap iteration is reduced to a single point (score) for each criterion. A threshold is established for each criterion using the evolution of the score for the base case. Only when the correlation between the bootstrapped factor and its base case factor was noticeably higher than that of the bootstrapped factor to another base case factor were the bootstrapped runs maintained for final mapping.

A significance level p from a t-test was selected to further assess the statistical significance of the chosen threshold. The findings were evaluated using a low p-value of 0.05, and the BS mapping for each base factor time-series criterion was then given. Due to random resampling (bootstrapping) and the random a-value for constrained factors, numerous solutions exist at various time points, allowing us to assess the rotational and statistical uncertainty of the averaged PMF solution. The averaged PMF solution's linear fit through zero between each point's standard deviation and its corresponding time point's mean defines this uncertainty. The slope of the linear fit, which was previously mentioned, determines the reported uncertainty (in percentage terms) for each component and is described in detail in supplementary section S3. The 500 bootstrapping runs were performed for the 8-factor solution at U-IGP1 and U-IGP2, and for the 7-factor solution at C-IGP1. Further results are described in section 3.2, while detailed description of the result is provided in supplementary section S3.

2.5 Back trajectory analysis using potential source contribution function (PSCF)

PSCF is a commonly used technique in atmospheric sciences to identify potential sources of air pollution. The PSCF model employs conditional probabilities to estimate the probability of air pollution originating from a specific grid cell and being transported to a receptor site. Specifically, PSCF calculates the probability that a trajectory will cross a particular grid cell, with a higher probability

https://doi.org/10.5194/egusphere-2024-1385
Preprint. Discussion started: 12 July 2024

indicating that the cell has a greater potential to be a source region of pollution. By analyzing the conditional probabilities for each grid cell, the PSCF model provides insight into the source contributions to the receptor site and can facilitate the development of targeted pollution control measures. The contribution function is determined by an arbitrary criterion value C (typically 50 to 90% of the highest concentration). The contribution value of an endpoint on a back trajectory with a receptor concentration greater than C is 1, else it will be 0, the multisite PSCF model is defined as:

$$p_{s,I} = \begin{cases} 1 & c_{s,I} \geq C_s \\ 0 & c_{s,I} < C_s \end{cases}$$

C_s: Criterion value of site

$p_{s,I}$: Result of conditional value for trajectory I from site s

$c_{s,I}$: Receptor concentration of back trajectory I from site s

$$PSCF_{ij} = \frac{\sum_{S=1}^{S} \sum_{I=1}^{L_S} p_{s,I}.\tau_{i,j,s,I}}{\sum_{S=1}^{S} \sum_{I=1}^{L_S} \tau_{i,j,s,I}} \quad (6)$$

$PSCF_{ij}$: PSCF value of grid i, j (latitude, longitude)

S : Total site number

L_S: Total back trajectory line number from site s

$\tau_{i,j,s,I}$: Endpoint number of back trajectory I from site s in grid i, j

In this study, 120 h (5 days) backward air mass trajectories arriving at the sampling site were computed. Back trajectory analysis was performed by (Hybrid Single Particle Lagrangian Integrated Trajectory v4.1 (HYSPLIT) (Draxler, 2020) software using Global data assimilation system (GDAS) meteorological files as inputs for the backward trajectory computation. The backward trajectories were computed every three hours (ending at 00:00, 03:00, 06:00, 09:00, 12:00, 15:00, 18:00, and 00:00 UTC) for each day of the period of study at 500 m above ground level. All height over 1500m were filtered out as it was assumed that air masses at this height will not affect ground level observations. The time series of all sites were combined to a single PSCF run. Openair was used to plot the PSCF graphs which operates in R (Carslaw, 2019).

https://doi.org/10.5194/egusphere-2024-1385
Preprint. Discussion started: 12 July 2024

3 Results and discussion

3.1 Mass composition of elements

Sub-hourly average El-$PM_{2.5}$ concentrations were measured, for which Fig. 2a, b and c (also Table S2) summarize the results of elements measured at all three sites. The elemental data was further subdivided into the warm and cold period to explore the role of factors (meteorology, formation mechanisms (especially sulfur and chloride) and their emission sources) that influence the variation of elements and their sources. The summary of the elemental concentration during warm and cold period is provided in Table S2.

The measured elemental concentrations during both periods at two sites in the U-IGP region were nearly identical (at U-IGP1: 19.2 $\mu g.m^{-3}$ in warm; 22.9 $\mu g.m^{-3}$ in cold) and U-IGP2: 17.4 $\mu g.m^{-3}$; 19.2 $\mu g.m^{-3}$). When comparing with the higher concentration at U-IGP1 to the C-IGP1 (12.6 $\mu g.m^{-3}$; 13.5 $\mu g.m^{-3}$), it was 1.5-1.7 times greater. During the colder period, when compared with a study conducted by Rai et al. (2021b), in U-IGP, revealed that measured concentrations at Delhi (32 $\mu g.m^{-3}$) were three times higher than those observed at the other sites globally (Beijing, Krakow, and London). When comparing the C-IGP region (this study) concentrations with both the U-IGP (as per this study) and the other three sites (study by Rai et al. (2021)), it was found that although the C-IGP concentrations were lower than those in the U-IGP, they were significantly higher than the mean concentration measured in Beijing (2.6 times), Krakow (3.1 times), and London (15 times). The high concentrations in the C-IGP region underscores the need for policymakers and scientists to direct their attention not only towards the U-IGP regions but also towards comprehensively characterizing the PM (particularly elements) in other downwind areas of the IGP regions.

Across the IGP regions, S, Cl, and K were the predominant contributors, accounting for over 83% of the El-$PM_{2.5}$ (elemental part of PM2.5) during the cold period (Fig. 2). In the warm period, these elements contributed over 73% in the U-IGP region, while in the C-IGP region, their contribution was 52% (which increased to 78% with the inclusion of Si). All of these elements are associated with combustion-related sources such as power plants, garbage, PVC, and crop burning (Gani et al., 2018; Shukla et al., 2021; Rai et al., 2020; Nalbandian, 2012). In both the IGP regions, during the warm

https://doi.org/10.5194/egusphere-2024-1385
Preprint. Discussion started: 12 July 2024

period, S and Cl decreased by a factor of 2 compared to the cold. The elevated levels of S and Cl during the cold period can be attributed to increased anthropogenic combustion activities in addition to conventional sources, that occur during winter, along with favorable meteorological conditions. We also examined the variations between the IGP regions and found that the mean concentration of El-$PM_{2.5}$ in the U-IGP region was 1.5 times higher than in the C-IGP region. When comparing the mean concentrations of all the elements, we observed that the C-IGP region generally had lower concentrations, except during the cold period where K and Rb were enhanced at the C-IGP1 (Fig. 2 (c)).

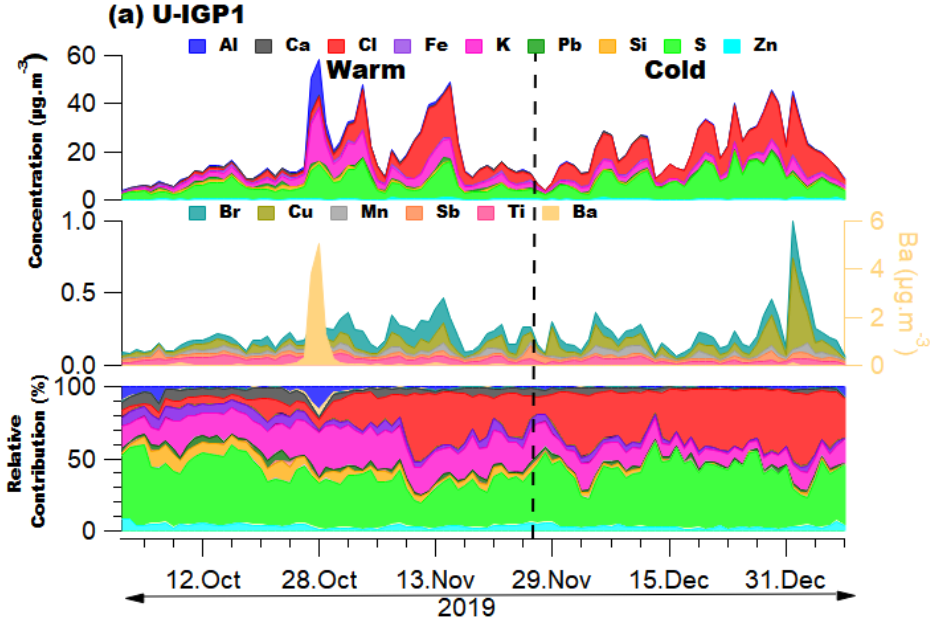

https://doi.org/10.5194/egusphere-2024-1385
Preprint. Discussion started: 12 July 2024

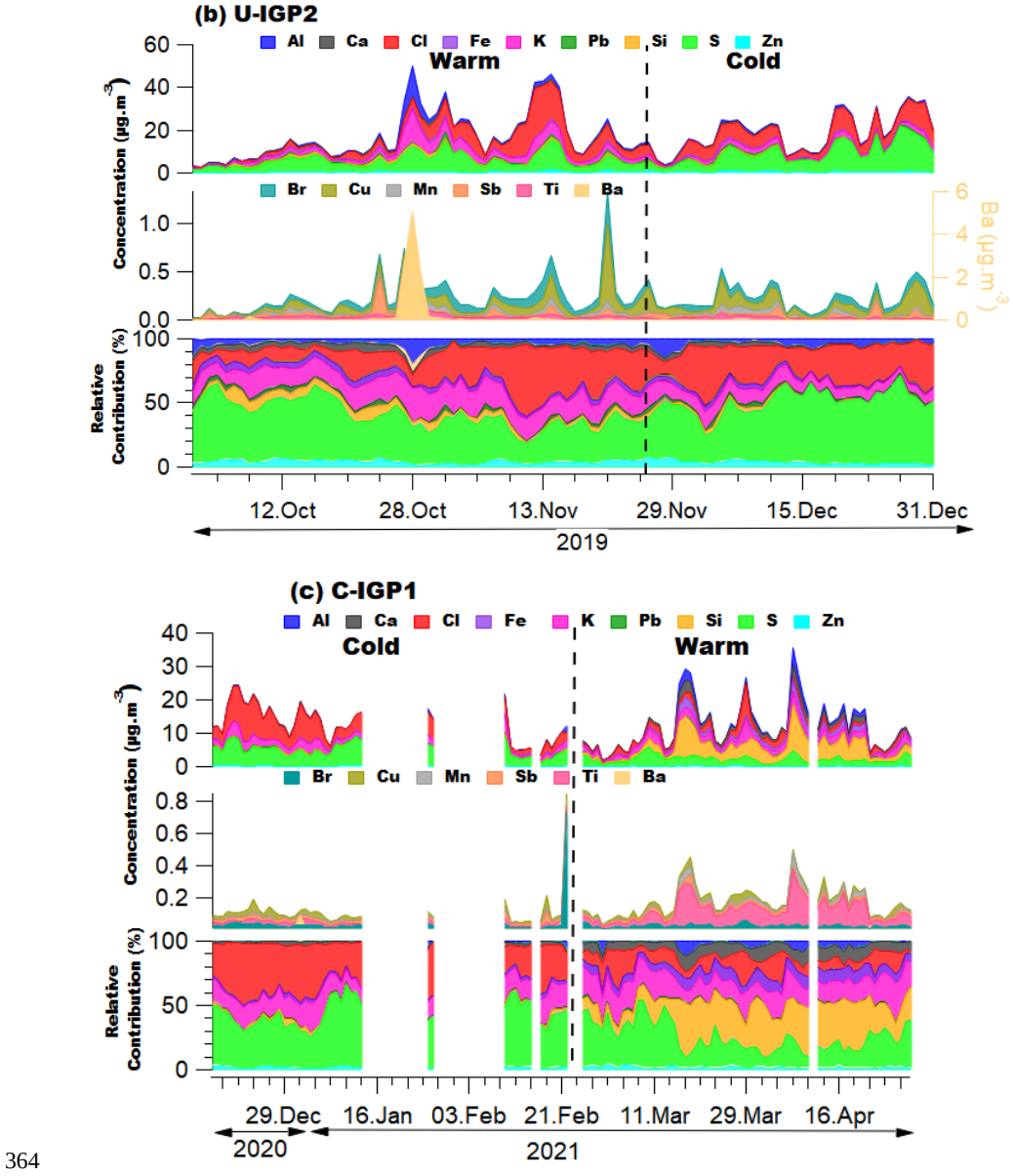

Figure 2. Time series of elemental concentration measured by Xact and RC of elements at (a) U-IGP1 and (b) U-IGP2 and (c) C-IGP1 sites.

3.2 Enrichment factor analysis and health impacts of elements

For the initial evaluation of the impact of human-caused emissions on atmospheric elemental levels, the enrichment factor (EF) was calculated for each observed element, utilizing Ti as a reference element (Majewski and Rogula-Kozłowska, 2016; Fomba et al., 2013). The calculation of EFs and crustal

https://doi.org/10.5194/egusphere-2024-1385
Preprint. Discussion started: 12 July 2024

contributions in elemental concentrations is provided in detail in supplementary section S4. The elements Al, Si, Fe, and Zr consistently exhibited EF values ranging from 0.4 to 2 (Fig. S14), indicating their association with crustal sources throughout the IGP regions and periods. Conversely, the EF values for K, Cr, Mn, and Ni fell within the range of 2 to 20 (Fig. S14), suggesting a combined influence of both crustal and anthropogenic sources on these elements throughout all the sites and periods. On the other hand, the elements S, Cl, Cu, Zn, As, Se, Br, Cd, Sn, Sb, and Pb demonstrated EF values exceeding 20, indicating a significant anthropogenic impact on these elements. The detailed results are discussed in the supplementary section S4.

The concentrations of carcinogenic elements, such as lead (Pb), nickel (Ni), arsenic (As), and chromium (Cr), in the atmosphere play a crucial role in determining the potential health risks for residents. Comparing with the standards by the International Agency for Research on Cancer (IARC, 2020), the average concentrations of these elements are below the inhalation reference concentrations (RfCs) recommended by the US Environmental Protection Agency (EPA) for residential air (0.2, 0.02, 0.015, and 0.1 $\mu g.m^{-3}$, respectively; USEPA, 2020), except for Pb. The exceedance of the mean concentration of Pb was higher at U-IGP1 (2.1-2.5) compared to U-IGP2 (1.9-2.2), with almost similar exceedances observed during warm periods as compared with cold at both the U-IGP. The exceedance of the mean concentration of other three elements were under the RfCs in the U-IGP, while all the four elements were below the RfCs in the C-IGP region during both periods.

https://doi.org/10.5194/egusphere-2024-1385
Preprint. Discussion started: 12 July 2024

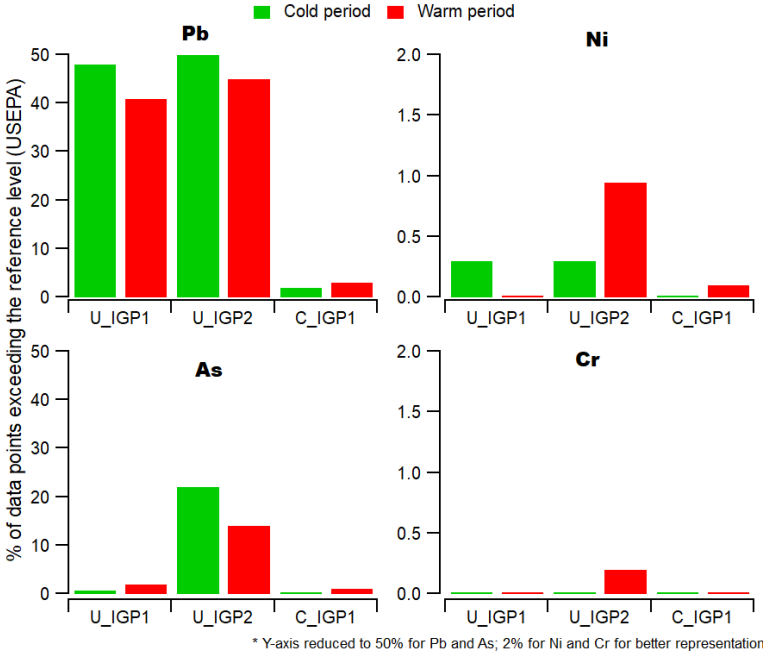

390 Figure 3. Individual exceedance percentage for each of the carcinogenic elements (Pb, Ni, As and Cr) during 2 periods and at the three sites.

392

However, when examining individual exceedances, the percentage of data points exceeding the 394 recommended RfCs set by the US EPA for Pb was very high (41 to 50% during both the periods in the U-IGP) as compared with other carcinogenic elements (Fig. 3). These observations indicate a serious 396 concern for human health, as lead can have critical effects on our nervous system, kidneys, immune system, and reproductive system (Mitra et al., 2022; Wani et al., 2015). Additionally, it can negatively 398 impact children, leading to behavioral problems, learning deficits, and decreased intelligence (Al osman et al., 2019; Reyes, 2015; Sanders et al., 2009). The exceedance of other carcinogenic element As was 400 found to be 10-32% at U-IGP2 during both periods. While, Ni and Cr had a lower percentage of data points exceeding the RfCs, generally remaining below 1% (Fig. 3). A different trend of high exceedance 402 of potentially harmful levels of carcinogenic elements were identified during warm periods (Pb at C-IGP1; Ni & As at both U-IGP2 & C-IGP1 sites ; Cr at U-IGP2 only, and C-IGP1). These findings 404 indicate that although the concentration of carcinogenic elements may be higher during cold period due

https://doi.org/10.5194/egusphere-2024-1385
Preprint. Discussion started: 12 July 2024

to accumulation of pollutants because of low boundary layer, but the individual exceedances can also be higher during warm and hence equally harmful to public health even during warm.

3.3 Elemental source apportionment (SA)

The source apportionment (SA) of elements using high time resolution El-$PM_{2.5}$ measurements using Xact was conducted at the three sites in the IGP region. Based on the characteristics and correlation among source profiles (as discussed in detail in supplementary section S2 (Table S5)), similar resolved sources were identified, including Cl-rich, coal combustion, Cu-rich, dust, SFC1, SFC2, and S-rich, across all three sites.

Variations in sources from warm to cold period were investigated for all three sites (two sites in U-IGP and one in C-IGP) and the data is obtained from Shukla et al. (2024). The process of selecting the optimal solution is described in detail in supporting information S1 (Text S1). The characteristics of the resolved factors will be discussed in subsequent sections, as well as in supplementary section S2. The bootstrapping analysis revealed that out of the 500 bootstrap runs, 100% of runs met the criteria at U-IGP1, 97% at U-IGP2, and 90% at the C-IGP1. Additionally, the PMF error for each factor was evaluated, and it was found to be less than 10% for all factors at all three sites, except for Cu-rich at U-IGP2 (14%) and C-IGP1 (26.5%), as well as coal combustion at C-IGP1 (32.5%). Detailed results of the bootstrapping analysis are provided in the supplementary section S3.

3.3.1 Variation of elemental sources during warm and cold

U-IGP region: At the U-IGP1, significant differences were observed in the RC of the elemental sources. The contribution of SFC1 (25 to 9%) and dust (12 to 5%) sources decreased significantly from the warm to cold period (Figs. 4 and 5). In contrast, the contribution of Cl-rich (28 to 44%) and S-rich (22 to 31%) sources increased compared to the warm period (Figs. 4 and 5). These differences indicate the influence

https://doi.org/10.5194/egusphere-2024-1385
Preprint. Discussion started: 12 July 2024

of meteorology during different periods, which will be discussed in detail in section 3.4. The

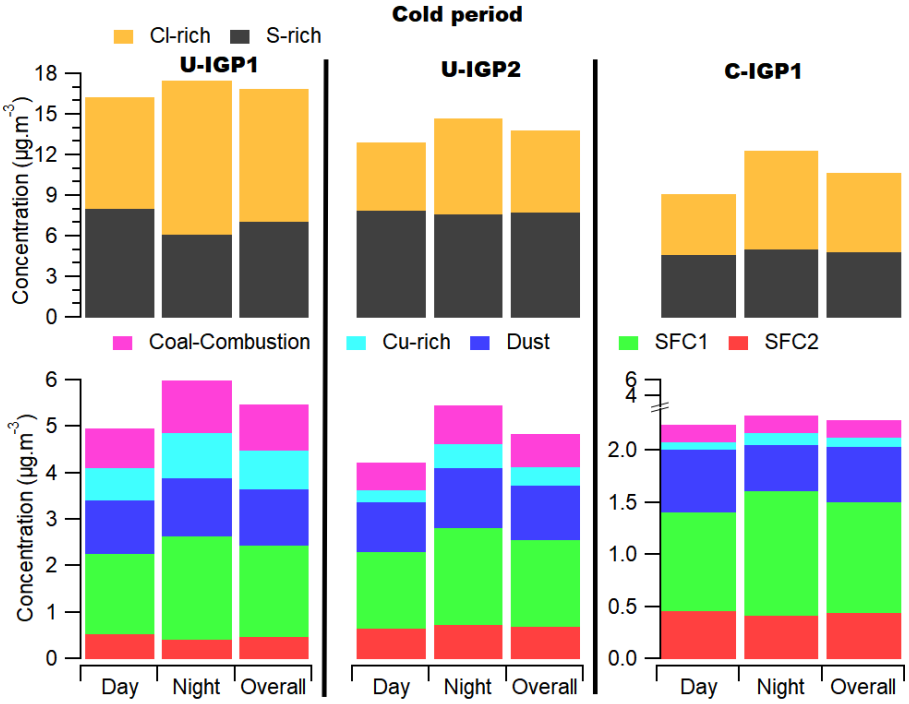

Figure 4. Variation in composition (µg.m^{-3}) of elemental sources at the three sites in the IGP region; U-IGP1, U-IGP2 and C-IGP1 between day, night and overall period during Cold.

absolute concentration of SFC1 and dust decreased by a factor of 2 and 1.6, respectively, while the concentrations of Cl-rich and S-rich increased by a factor of 2 each (Fig. 5). The increased Cl-rich and S-rich during cold can be due to the high RH conditions favour the fast formation of these sources through aqueous phase reactions.

At U-IGP2, there was a similar variation as observed for the U-IGP1. Cu-rich and coal combustion sources exhibited minimal variation from warm to cold periods, indicating a consistent emission source irrespective of the season such as industries. The warm/cold ratio for the average concentration of SFC1, dust, Cu-rich, S-rich, Cl-rich and coal combustion, was 1.7, 1.3, 1.2, 1.2, 0.8 and 0.4 respectively. At U-IGP a similar night/day ratio for average concentrations was found for Cu-rich (2-2.6), followed by

https://doi.org/10.5194/egusphere-2024-1385
Preprint. Discussion started: 12 July 2024

Cl-rich (1.4-1.7), coal combustion (1.4-1.7), dust (1.2-1.3), SFC1 (1.1-1.3), and SFC2 (1.1) (summarized in Table S3) during both periods. Only the S-rich concentration during the warm period exhibited higher daytime concentrations by a factor of 1.2 compared to night, indicating the role of photochemical formation influenced by high solar radiation (Fig. S3). The average concentration of the S-rich source was nearly equal during both day and night in the cold period, which may be attributed to the role of aqueous phase oxidation occurring at night during the cold period, while it was absent during the warm period (Fig. 4).

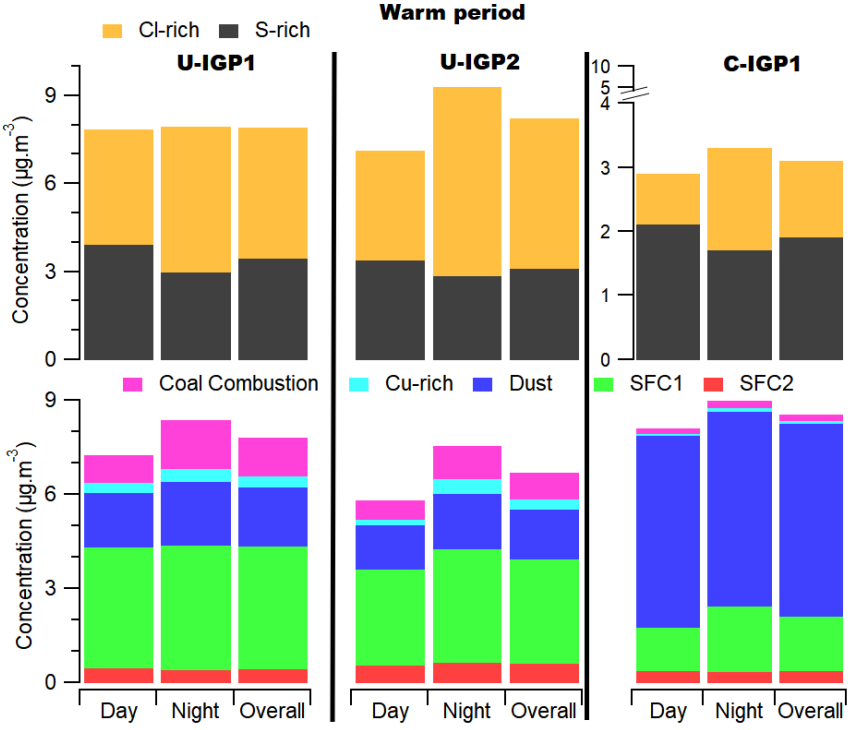

Figure 5. Variation in composition (µg.m^{-3}) of elemental sources at the three sites in the IGP region; U-IGP1, U-IGP2 and C-IGP1 between day, night and overall period during Warm.

C-IGP region: At the C-IGP1, there was a significant decrease in the RC of the dust source, dropping from 52% to 4% (Fig. S16). The ratio of average concentration from warm to cold was 11. This substantial difference observed exclusively at the C-IGP1 can be attributed to the occurrence of multiple

https://doi.org/10.5194/egusphere-2024-1385
Preprint. Discussion started: 12 July 2024

dust storms during the warm period (prominent on 07, 08, 13 and 21 April (Fig. S9)), while the concentration during the cold periods was primarily due to road dust resuspension (the diurnal (Fig.6) is similar with peak traffic hours). The warm/cold ratio of the average concentration for SFC1, SFC2, Cl-rich, S-rich, Cu-rich, and coal combustion are 1.6, 0.8, 0.2, 0.4, 0.8, and 1.2, respectively (Figs. 4 and 5). The S-rich and Cl-rich sources exhibited similar variations from the warm to cold period, showing similar patterns observed at the U-IGP sites and thus indicate the regional characteristics of the sources and can be attributed to favorable meteorological conditions during the cold period, as well as additional anthropogenic heating emissions, explored in further sections.

During the warm period, SFC1, Cl-rich, Cu-rich, coal combustion, and dust showed higher average concentrations at night compared to daytime, with night/day ratios of 1.5, 2, 2.3, 1.2, and 1.02, respectively (Figs. 4 and 5). On the other hand, SFC2 and S-rich had higher concentrations during the day by factors of 1.1 and 1.2, respectively. In the cold period, a similar trend in day-to-night variations was observed for Cl-rich, S-rich, and Cu-rich, but the opposite trend was observed for SFC1, SFC2, coal combustion, and dust. However, the difference in mean concentration from day to night was much lower during the cold period compared to the warm period (Fig.5). The dust source exhibited higher concentrations at night (with an average night concentration to day concentration ratio of 1.8) only during the cold season, as the dust source was primarily attributed to road dust suspension, which is higher at night when the entry restrictions of HDV are lifted.

3.3.2 Diurnal variation of elemental sources

Significant diurnal differences in source patterns were noted between warm and cold periods across the IGP regions (Fig. 6). Daytime SFC1 concentration was higher in the warm period, while favorable meteorological conditions during the cold period, such as low boundary layer height and calm wind speeds along with increased heating activities, led to higher nighttime concentrations. SFC2, associated with industrial waste burning, peaked early in the morning in both IGP regions during both periods. High chlorine concentrations peaked between 6:00 LT and 8:00 LT in both IGP regions (Fig. 6), attributed to the semi-volatile nature of ammonium chloride, converting to a gaseous form with rising temperatures. A distinct diurnal pattern in Cl-rich variation was observed between warm and cold

https://doi.org/10.5194/egusphere-2024-1385
Preprint. Discussion started: 12 July 2024

periods. During the warm period, Cl-rich concentrations began to increase around 8:00 PM, while during the cold period, they started to rise around 4:00 PM. During the warm period, both IGP regions showed high afternoon concentrations of S-rich source, with U-IGP1 having the highest, followed by U-IGP2 and C-IGP1. However, distinct diurnal patterns emerged during the cold period in both regions. U-IGP2 and C-IGP1 exhibited increased nighttime concentrations, suggesting potential sulfate formation via aqueous phase oxidation of SO2 by NO2 under high RH conditions, contributing to new particle formation. Further details on diurnal variations of other sources are discussed in supplementary section S5.

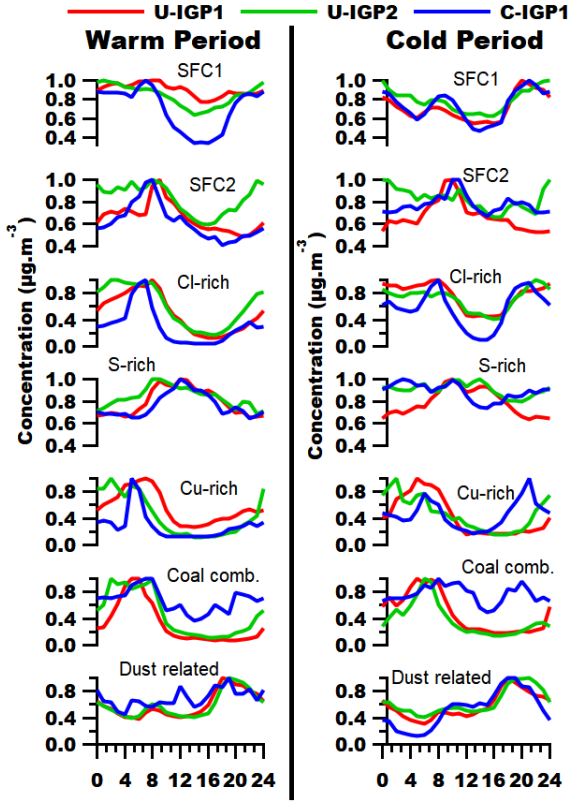

Figure 6. Normalised diurnal variation of elemental sources at the three sites in the IGP region; U-IGP1, U-IGP2 and C-IGP1 during the warm and cold periods.

3.3.3 Spatial variation of elemental sources

In this section, we have observed variations in the elemental sources first within the U-IGP region (between the two sites in the U-IGP) and then between the U-IGP and the C-IGP region. Within the U-

https://doi.org/10.5194/egusphere-2024-1385
Preprint. Discussion started: 12 July 2024

IGP region, during the warm period, Cl-rich (28.3-34.2%) dominated the sources at both sites, followed by SFC1 (28.3-34.2%), S-rich (21-22%), dust (10.6-12%), coal combustion (5.7-7.8%), SFC2 (2.9-4.1%), and Cu-rich (2.1-2.4%) (Fig. S16). A similar pattern of source contribution was observed within the U-IGP sites during the cold period, with an increased RC from Cl-rich and S-rich, while the contribution from other sources decreased. The difference in average concentration between the sites was minimal during the warm period, but it increased sharply during the cold period, indicating the role of increased local (site specific) anthropogenic emission sources as well as dilution of transported sources as U-IGP2 is upstream of the U-IGP1 (Fig. 1). The remaining sources exhibited similar variations in day and night concentrations at both sites during both periods and are discussed in supplementary section S6.

When comparing the variations between the U-IGP and C-IGP regions, it was found that the RC of sources followed the same sequence in both regions, with Cl-rich, S-rich, and SFC1 dominating the sources, except for the dust source at C-IGP1 during the warm period due to several dust storms as already discussed in previous section. During the cold period, the dust source was comparable in the two IGP regions, as only road dust resuspension contributed at all the sites, as shown in the diurnal pattern (Fig. 6). There was a significant variation in the average concentrations between the U-IGP and C-IGP regions during the warm period. The concentrations of SFC1, SFC2, Cl-rich, S-rich, Cu-rich, coal combustion, and dust were lower on average at the C-IGP compared to the U-IGP sites by factors of 2.2, 1.5, 4, 1.7, 4.8, 5.1, and 0.3, respectively. Cl-rich, Cu-rich, and coal combustion were considerably higher in the U-IGP region compared to the C-IGP during the warm period, indicating a greater influence of industrial emissions in the U-IGP region (Fig. 1). Multi-site PSCF plots for Cl-rich pollutants revealed distinct source regions (Fig. 7). In the warm period, primary source regions were mainly in the northeast of U-IGP sites and from the north at C-IGP1. Conversely, during the cold period, Cl-rich pollutants predominantly originated from the northwest within the IGP regions. There are several steel manufacturing industries in both the regions Punjab and Haryana as well as Moradabad (Rai et al., 2020). Origin regions of SFC1 varied noticeably, with northern contributions in the warm period and northwest and east directions in the cold period (Fig.6). The PSCF plots of the other sources are shown in Fig. S6 of supplementary.

https://doi.org/10.5194/egusphere-2024-1385
Preprint. Discussion started: 12 July 2024

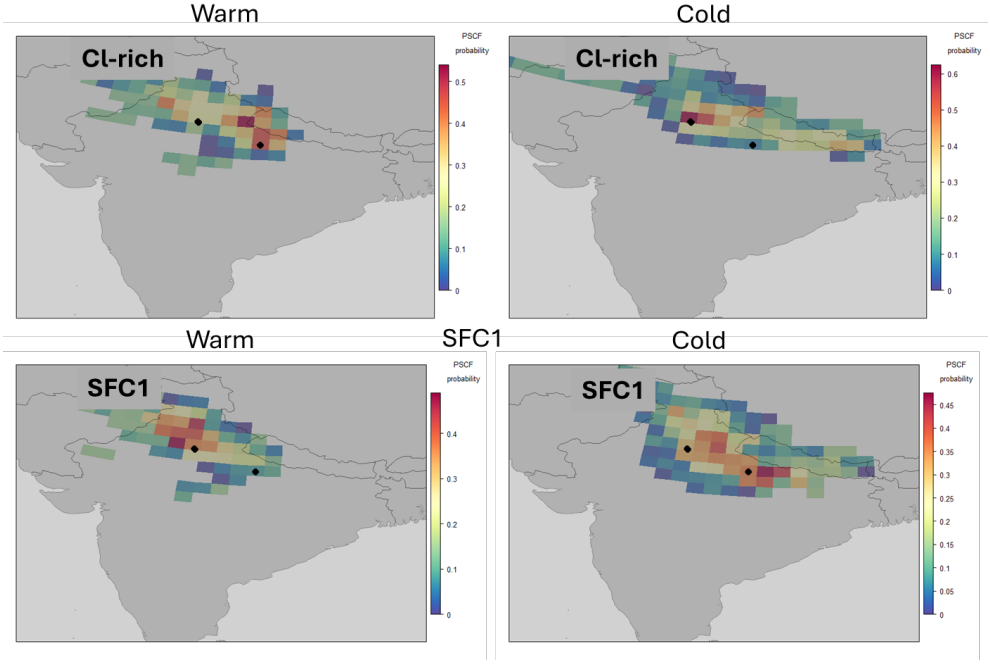

524 Figure 7. PSCF plot for multi-site (using three IGP sites elemental sources data) for the warm and cold
period of the Cl-rich and SFC1 sources (PSCF plot for rest of the sources are shown in Fig. S4).

526 During the cold period, the ratios of average concentration at the U-IGP to the C-IGP (U-IGP/C-IGP)
significantly reduced. The ratios for SFC1, SFC2, Cl-rich, S-rich, Cu-rich, coal combustion, and dust
528 were 1.8, 1.3, 1.1, 1.6, 6.6, 5, and 2.3, respectively. Origin regions of SFC1 varied noticeably, with
northern contributions in the warm period and northwest and east directions in the cold period (Fig.7).
530 There was a significantly higher increase in Cl-rich at the C-IGP compared to the U-IGP from the warm
to cold period. Similarly, dust also decreased significantly from the warm to cold period at the C-IGP,
532 with a U-IGP/C-IGP ratio of 2.3 during the cold period. The other industrial sources, Cu-rich, and coal
combustion, were also significantly higher in concentration at the U-IGP sites, indicating a lesser
534 influence of industries in the C-IGP region compared to the U-IGP region.

3.4 Role of meteorology and pollution episodes of elemental sources

536 Throughout both periods, there were frequent instances of high pollution (with the average daily
concentration of PM2.5 reaching six times the NAAQS of 60 µg.m−3). We observed two distinct
538 episodes of pollution each during the warm (EP1 and EP2) and cold (EP3 and EP4) periods,

https://doi.org/10.5194/egusphere-2024-1385
Preprint. Discussion started: 12 July 2024

characterized by unique meteorological conditions (Fig. 3), as well as distinct emission sources that significantly elevated the levels of PM2.5 when compared to clean periods (two clean periods were also identified during both the warm and cold periods to make comparisons with their respective pollution episodes). The durations of these episodes are outlined in Table S6. During both warm (C1) and cold (C2) clean periods at both U-IGP sites, the average concentration of $PM_{2.5}$ remained relatively low, around 43 $\mu g.m^{-3}$. A detailed discussion about the variation of sources during clean period in supplementary section S7.

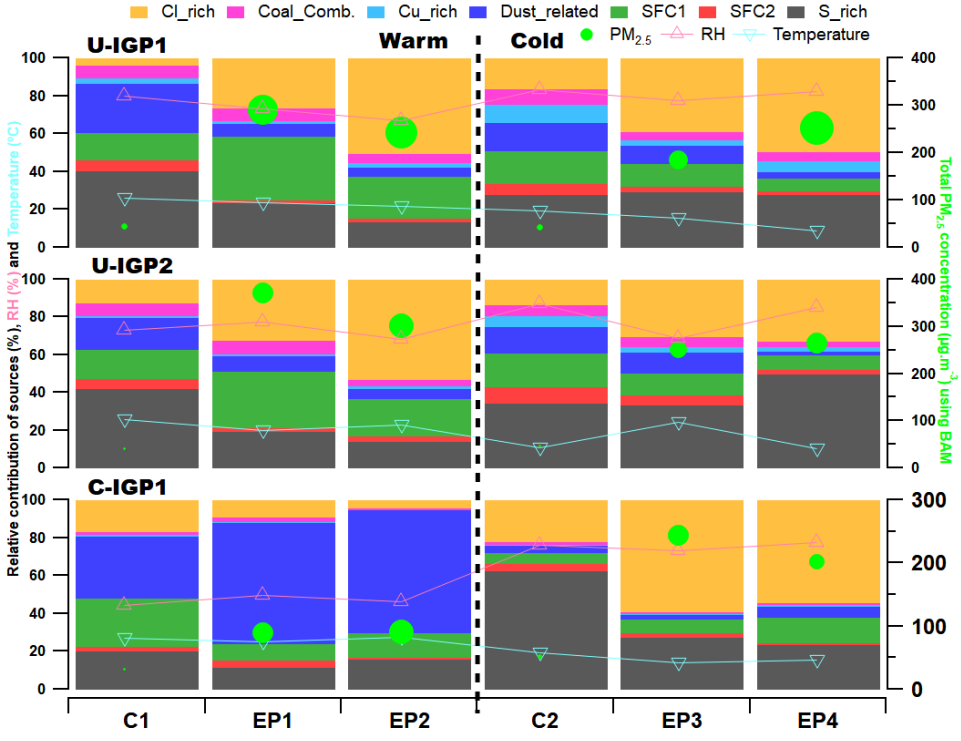

Figure 8. The variation in the RC of elemental sources, $PM_{2.5}$, RH and Temperature during the clean and polluted episodes C1, EP1, EP2, C2, EP3 and EP4 during both warm and cold period

The rise in $PM_{2.5}$ concentrations corresponded to an elevation in elemental concentrations from the clean period (C1), to EP1 and EP2. Across all three sites in the IGP region, this increase ranged from 3.9 to 5.6, suggesting a substantial influence on the elemental composition of $PM_{2.5}$. During C1, S-rich and dust sources were the dominant contributors at all three sites. However, during C2, S-rich and Cl-

https://doi.org/10.5194/egusphere-2024-1385
Preprint. Discussion started: 12 July 2024

rich sources took precedence, emphasizing the impact of meteorological conditions and dynamic emission sources. There was also a distinct pattern of diurnal variation at C-IGP during C2 as compared to all sites during C1 and C2 (Fig.9), mostly the diurnal concentration was high during afternoon, but during C2 at C-IGP1, the high concentration of S-rich extended beyond the noon till mid-night, indicating the role of other formation mechanism (aqueous phase oxidation) during the period.

Analyzing the change in elemental sources from C1 to EP1, we observed a significant increase in the RC of Cl-rich, with a rise of 23% at U-IGP1 (average concentration increased by a factor of 39) and 20% at U-IGP2 (average concentration increased by a factor of 14.2) (Fig. 8). SFC1 also exhibited substantial growth, with an 18% increase at U-IGP1 (average concentration increased by a factor of 12) and a 14% increase at U-IGP2 (average concentration increased by a factor of 11). Despite a decrease in the RC of S-rich by 18% at U-IGP1 and 20% at U-IGP2 (Fig. 8), the average concentrations still saw significant increases by factors of 3.1 and 2.7, respectively (Table S4). During EP1 at U-IGP, we observed a prominent pollution event caused by crop residue burning, as documented in previous studies (Lalchandani et al., 2022; Shukla et al., 2023; Manchanda et al., 2022), specifically during the last week of October.

At C-IGP1, a distinct change in elemental sources occurred during the warm period from C1 to EP2. The dust source displayed a remarkable increase of 32% in RC, leading to an average concentration increase by a factor of 9. Conversely, the RC of the SFC1 source decreased by 12%, while the average concentration increased by a factor of 2 (Fig.8), there was a clear sharp peak around 7:00 LT (Fig. 9). These findings further support the influence of agricultural residue burning in the IGP region, which impacted both the U-IGP and C-IGP during EP2 (Bray et al., 2019; Lan et al., 2022).

https://doi.org/10.5194/egusphere-2024-1385
Preprint. Discussion started: 12 July 2024

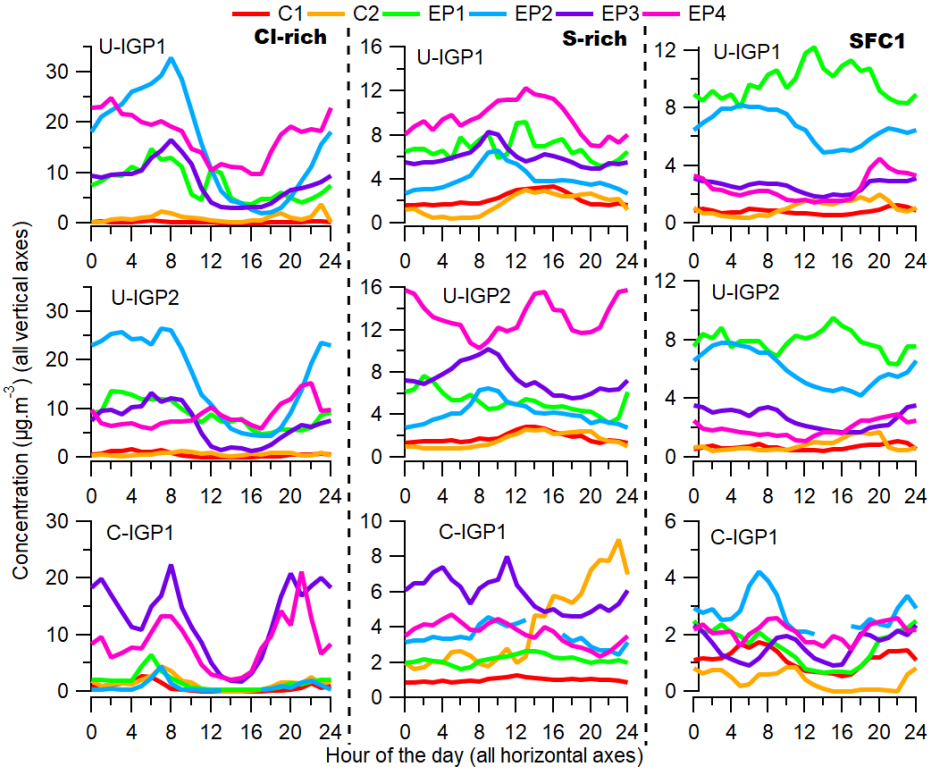

Figure 9. The diurnal variation of Cl-rich, S-rich and SFC1 sources having major role in the variation of El-$PM_{2.5}$ during the clean and polluted episodes C1, EP1, EP2, C2, EP3 and EP4 during both warm and cold period.

For the cold period, the $PM_{2.5}$ increased from C2 to EP3 and EP4 by a factor ranging from 3.9 to 6, similarly the elemental average concentration increased from C2 to EP3 and EP4 by a factor ranging from 2.7 to 5.6 at all the three sites of the IGP region. During the cold period, there was a remarkable surge in both $PM_{2.5}$ and El-$PM_{2.5}$ concentrations across the IGP region, specifically from C2 to EP3 and EP4. The concentration levels exhibited a significant increase, with factors ranging from 3.9 to 6 for $PM_{2.5}$ and 2.7 to 5.6 for El-$PM_{2.5}$ at all three IGP sites. Notably, the U-IGP1 experienced the most pronounced changes during EP4. Analyzing the variation in elemental sources during the cold period's pollution episodes (EP3 and EP4), Cl-rich particles emerged as key contributors to the elevation of El-$PM_{2.5}$. Recent observations in U-IGP have shown increased levels of chloride concentrations, particularly during nocturnal haze. This suggests that chloric acid may play a role in supporting particle growth under low-temperature and high-humidity conditions (Gunthe et al., 2021; Mishra et al., 2023).

https://doi.org/10.5194/egusphere-2024-1385
Preprint. Discussion started: 12 July 2024

At U-IGP1, the RC of Cl-rich particles witnessed a surge of 22% during EP3 and 33% during EP4, can be also observed in Fig.8. U-IGP2 displayed an increase of 16% during EP3 and 19% during EP4, while C-IGP1 exhibited a substantial rise of 37% during EP3 and 32% during EP4. These findings align with the observed significant changes in RC (Fig. 8). The diurnal shown in Fig. 9 shows a distinct behavior in U-IGP where the Cl-rich was higher during pollution episode during warm (EP2), while at C-IGP it was higher during cold period (EP3 and EP4).

Moreover, the average concentration of the Cl-rich source has a 17-fold increase at U-IGP1 and a notable 13-fold increase at U-IGP2, while C-IGP1 displayed the most pronounced increase of 9 times during EP3. These enhancements in concentration further reinforce the impact of Cl-rich particles on El-$PM_{2.5}$ levels. While the RC of S-rich particles exhibited a declining trend (excluding EP3 at U-IGP1 and EP4 at U-IGP2), the average concentration showed a contrasting rise during EP3 and EP4. At the U-IGP, diurnal variations of S-rich compounds exhibited afternoon peaks during both EP-3 and EP-4, contrasting with a relatively flat low increase during C2. Conversely, at the C-IGP, S-rich emissions demonstrated a sharp increase from 12 noon to midnight during C2, whereas during EP-3 and EP-4, two morning peaks were observed at 3:00 LT and 11:00 LT (Fig. 9). The concentration levels soared, with factors ranging from 3.3 to 5.3 at U-IGP1, 4.4 to 7.7 at U-IGP2, and 1 to 1.5 at C-IGP1 compared to the clean period. These shifts indicate a complex interplay between source dynamics and El-$PM_{2.5}$ concentrations during pollution episodes. Furthermore, other elemental sources did not demonstrate significant changes in RC from C2 to EP3 and EP4. However, the average concentration of SFC1 witnessed a substantial increase. At U-IGP1, it doubled, while at U-IGP2, it surged by 2.1 to 2.9 times, and at C-IGP1, it multiplied by 4 to 5.3 times. These findings suggest an intensified influence of solid fuel combustion for heating purposes, particularly during colder temperatures. Moreover, the concentrations of Cu-rich and coal combustion sources exhibited a striking three-fold increase at U-IGP1. This surge can be attributed to the burning of e-waste, which contains copper. At the U-IGP2, coal combustion displayed a factor of 4.4 increase during EP3 and 2.7 increase during EP4 compared to C2. These findings shed light on the complex dynamics of elemental sources and their impact on pollution episodes during the cold period.

https://doi.org/10.5194/egusphere-2024-1385
Preprint. Discussion started: 12 July 2024

4 Conclusion

In this study the high-time resolution elemental composition of particulate matter (El-$PM_{2.5}$) was observed in the Indo-Gangetic Plain region. The elemental concentrations measured at the two sites in the U-IGP region were similar during both warm and cold, highlighting the consistency of pollution levels in the area. However, it was observed that U-IGP1 exhibited higher concentrations compared to C-IGP1. During the cold period across IGP, S, Cl, and K as the major contributors to El-$PM_{2.5}$ and associated with combustion-related sources such as power plants, garbage, PVC, and crop burning, highlighting the substantial impact of anthropogenic activities on regional air quality. Elements such as Al, Si, Sr, and Ba showed a 3 to 10-fold increase during the warm period, indicating the influence of seasonal factors on pollution levels.

Enrichment factor analysis revealed valuable insights into the sources of pollution. While concentrations of carcinogenic elements (Pb, Ni, As, Cr) generally remained below recommended levels, lead concentrations exceeded the limits during warm periods in U-IGP. This finding raises concerns about human health as lead exposure even during warm, can lead to severe neurological, renal, immune, and reproductive effects. Further we identified elemental sources using ME-2 solver, including Cl-rich, coal combustion, Cu-rich, dust, SFC1, SFC2, and S-rich. SFC1 and Dust, showed a decrease in contribution during the cold period, while Cl-rich and S-rich sources increased. Meteorological conditions, especially during the cold period, were crucial in pollutant accumulation, with factors like low PBLH, low temperatures, and high relative humidity promoting pollutant retention and rapid sulfate formation through aqueous phase reactions, emphasizing the link between meteorology and pollution dynamics.

The diurnal patterns of sources differed between warm and cold periods. For example, during the warm period, the Cl-rich source had higher concentrations at night, indicating its formation due to condensation along with the role of low PBLH and its accumulation. Conversely, the S-rich source showed higher concentrations during the daytime, possibly due to photochemical sulfate formation. Variations in sources were observed within the U-IGP region and between the U-IGP and C-IGP regions, highlighting spatial variability. Cl-rich, S-rich, and SFC1 were dominant sources in both

https://doi.org/10.5194/egusphere-2024-1385
Preprint. Discussion started: 12 July 2024

regions. The U-IGP region showed higher concentrations of industrial-related sources, such as Cu-rich and coal combustion, compared to the C-IGP region, indicating a greater influence of industrial emissions. The multi-site PSCF analysis observed the role of regional transport and local emissions contributing to variations in source origin regions.

The escalation of PM2.5 concentrations throughout the Indo-Gangetic Plain (IGP) region during pollution episodes signifies a notable change in particulate matter's elemental composition. A significant increase in Cl-rich and SFC1 sources during pollution episodes, suggesting the impact of dynamic emission sources and agricultural residue burning. Furthermore, during cold periods, notable surges in Cl-rich particles emphasize their role in supporting particle growth under low-temperature and high-humidity conditions, highlighting the complex interplay between elemental sources and pollution dynamics.

Overall, this study highlights the complex nature of air pollution in the IGP, with multiple factors influencing the composition and characteristics of $PM_{2.5}$. The significant pollutant concentrations observed in the C-IGP region, compared to other sites, highlights the urgency for policymakers and scientists to expand their focus beyond the U-IGP regions. The findings underscore the need for targeted mitigation strategies, improved understanding of seasonal variations, and proactive measures to safeguard public health and mitigate the detrimental effects of air pollution in the region.

Data availability

The data used in this study can be found online at https://doi.org/10.5281/zenodo.12212768 (Shukla et al. 2024)

CRediT authorship contribution statement

Ashutosh K. Shukla: Methodology, Software, Validation, Formal analysis, Investigation, Writing - original draft, Writing - review & editing, Visualization. **Sachchida N. Tripathi:** Conceptualization, Writing - review & editing, Supervision, Project administration, Funding acquisition. **Shamitaksha Talukdar:** Methodology, Validation, Software, Validation, Formal analysis, Writing - review & editing. **Vishnu Murari:** Investigation, Data Curation, Writing - review & editing. **Sreenivas**

https://doi.org/10.5194/egusphere-2024-1385
Preprint. Discussion started: 12 July 2024

Gaddamidi: Investigation, Data Curation, Writing - review & editing. **Manousos-Ioannis Manousakas:** Formal analysis, Validation, Writing - review & editing **Vipul Lalchandani:** Investigation, Writing -review & editing. **Kuldeep Dixit:** Methodology, Validation, Writing -review & editing. **Vinayak M. Ruge:** Instrumentation, Writing - review & editing. **Peeyush Khare:** Validation, Writing - review & editing. **Mayank Kumar:** Resources, Writing - Review & Editing. **Vikram Singh:** Resources, Writing - Review & Editing. **Neeraj Rastogi:** Resources, Writing - review & editing. **Suresh Tiwari:** Resources, Writing - review & editing. **Atul K. Srivastava:** Resources, Writing - review & editing. **Dilip Ganguly:** Resources, Writing - review & editing. **Kaspar Rudolf Daellenbach:** validation, Writing - review & editing. **Andre. S. H. Prevot:** Formal analysis, Validation, Writing - review & editing

Competing interests

Vinayak M. Ruge is employed by Tesscorn Aerofluid Inc., which has the contract from the Cooper Environmental Services for the service and maintenance of the Xact® 625 in India.

Acknowledgements.

SNT gratefully acknowledge the financial support provided by Central Pollution Control Board (CPCB), Government of India to conduct this research under grant no. AQM/Source apportionment_EPC Project/2017 and the Swiss Agency for Development and Cooperation, Switzerland, to conduct this research under project no. 7F-10093. 01. 04 (contract no. 81062452). The authors would like to acknowledge the support from UPPCB (Uttar Pradesh Pollution Control Board) for the set-up of the campaign site at Lucknow. The SNT would like to acknowledge the support of PSI and Centre of Excellence (ATMAN) approved by the office of the Principal Scientific Officer to the Government of India. The CoE is supported by philanthropies including Bloomberg Philanthropies, the Children's Investment Fund Foundation (CIFF), the Open Philanthropy and the Clean Air Fund. SNT would also like to acknowledge J.C. Bose grant for their support in conducting this research under grant no JCB/2020/000044 AKS acknowledges Dr. T.V Ramesh Reddy for his help in processing of meteorological data.

https://doi.org/10.5194/egusphere-2024-1385
Preprint. Discussion started: 12 July 2024

References

Belis, C. A., Favez, O., Mircea, M., Diapouli, E., Manousakas, M. I., Vratolis, S., Gilardoni, S., Paglione, M., Decesari, S., Mocnik, G., Mooibroek, D., Salvador, P., Takahama, S., Vecchi, R., and Paatero, P.: European Guide on Air Pollution Source Apportionment with Receptor Models - Revised Version 2019, https://doi.org/10.2760/439106, 2019.

Bhat, M. A., Romshoo, S. A., and Beig, G.: Aerosol black carbon at an urban site-Srinagar, Northwestern Himalaya, India: Seasonality, sources, meteorology and radiative forcing, Atmos. Environ., 165, 336–348, https://doi.org/10.1016/J.ATMOSENV.2017.07.004, 2017.

Bray, C. D., Battye, W. H., and Aneja, V. P.: The role of biomass burning agricultural emissions in the Indo-Gangetic Plains on the air quality in New Delhi, India, Atmos. Environ., 218, 116983, https://doi.org/10.1016/J.ATMOSENV.2019.116983, 2019.

Brown, S. G., Eberly, S., Paatero, P., and Norris, G. A.: Methods for estimating uncertainty in PMF solutions: Examples with ambient air and water quality data and guidance on reporting PMF results, Sci. Total Environ., 518–519, 626–635, https://doi.org/10.1016/j.scitotenv.2015.01.022, 2015.

Canonaco, F., Crippa, M., Slowik, J. G., Baltensperger, U., and Prévôt, A. S. H.: SoFi, an IGOR-based interface for the efficient use of the generalized multilinear engine (ME-2) for the source apportionment: ME-2 application to aerosol mass spectrometer data, Atmos. Meas. Tech., 6, 3649–3661, https://doi.org/10.5194/amt-6-3649-2013, 2013.

Canonaco, F., Tobler, A., Chen, G., Sosedova, Y., Slowik, J. G., Bozzetti, C., Daellenbach, K. R., ElHaddad, I., Crippa, M., Huang, R.-J., Furger, M., Baltensperger, U., and Prévôt, A. S. H.: A new method for long-term source apportionment with time-dependent factor profiles and uncertainty assessment using SoFi Pro: application to one year of organic aerosol data, Atmos. Meas. Tech. Discuss., 1–39, https://doi.org/10.5194/amt-2020-204, 2020.

Carslaw, D. C.: The Openair Manual—Open-Source Tools for Analysing Air Pollution Data. Manual for version 2.6-5. University of York, 2019.

Cooper, J. a, Petterson, K., Geiger, A., Siemers, A., and Rupprecht, B.: Guide for Developing a Multi-Metals , Fence-Line Monitoring Plan for Fugitive Emissions Using X-Ray Based Monitors Guide for

https://doi.org/10.5194/egusphere-2024-1385
Preprint. Discussion started: 12 July 2024

726 Developing a Multi-Metals , Fence-Line Based Monitors, Cooper Environ. Serv. Portland, Oregon, 1–
42, 2010.
728 Das, A., Singh, G., Habib, G., and Kumar, A.: Non-carcinogenic and Carcinogenic Risk Assessment of
Trace Elements of PM 2.5 During Winter and Pre-monsoon Seasons in Delhi: A Case Study, Expo.
730 Heal., 12, 63–77, https://doi.org/10.1007/s12403-018-0285-y, 2020.
Dumka, U. C., Kaskaoutis, D. G., Mihalopoulos, N., and Sheoran, R.: Identification of key aerosol types
732 and mixing states in the central Indian Himalayas during the GVAX campaign: the role of particle size
in aerosol classification, Sci. Total Environ., 761, 143188,
734 https://doi.org/10.1016/J.SCITOTENV.2020.143188, 2021.
Fuller, R., Landrigan, P. J., Balakrishnan, K., Bathan, G., Bose-O'Reilly, S., Brauer, M., Caravanos, J.,
736 Chiles, T., Cohen, A., Corra, L., Cropper, M., Ferraro, G., Hanna, J., Hanrahan, D., Hu, H., Hunter, D.,
Janata, G., Kupka, R., Lanphear, B., Lichtveld, M., Martin, K., Mustapha, A., Sanchez-Triana, E.,
738 Sandilya, K., Schaefli, L., Shaw, J., Seddon, J., Suk, W., Téllez-Rojo, M. M., and Yan, C.: Pollution
and health: a progress update, Lancet Planet. Heal., 6, e535–e547, https://doi.org/10.1016/S2542-
740 5196(22)00090-0, 2022.
Gani, S., Bhandari, S., Seraj, S., Wang, D. S., Patel, K., Soni, P., Arub, Z., Habib, G., Hildebrandt Ruiz,
742 L., and Apte, J.: Submicron aerosol composition in the world's most polluted megacity: The Delhi
Aerosol Supersite campaign, Atmos. Chem. Phys. Discuss., 5, 1–33, https://doi.org/10.5194/acp-2018-
744 1066, 2018.
Geiger, A., Portland, J. C.-, Cooper, O., and 2010, undefined: Overview of airborne metals regulations,
746 exposure limits, health effects, and contemporary research, cooperenvironmental.com, 2010.
Gelaro, R., McCarty, W., Suárez, M. J., Todling, R., Molod, A., Takacs, L., Randles, C. A., Darmenov,
748 A., Bosilovich, M. G., Reichle, R., Wargan, K., Coy, L., Cullather, R., Draper, C., Akella, S., Buchard,
V., Conaty, A., da Silva, A. M., Gu, W., Kim, G. K., Koster, R., Lucchesi, R., Merkova, D., Nielsen, J.
750 E., Partyka, G., Pawson, S., Putman, W., Rienecker, M., Schubert, S. D., Sienkiewicz, M., and Zhao,
B.: The Modern-Era Retrospective Analysis for Research and Applications, Version 2 (MERRA-2), J.
752 Clim., 30, 5419–5454, https://doi.org/10.1175/JCLI-D-16-0758.1, 2017.
Giordano, S., Adamo, P., Spagnuolo, V., Tretiach, M., and Bargagli, R.: Accumulation of airborne trace

https://doi.org/10.5194/egusphere-2024-1385
Preprint. Discussion started: 12 July 2024

754 elements in mosses, lichens and synthetic materials exposed at urban monitoring stations: Towards a harmonisation of the moss-bag technique, Chemosphere, 90, 292–299,
756 https://doi.org/10.1016/J.CHEMOSPHERE.2012.07.006, 2013.

Gunthe, S. S., Liu, P., Panda, U., Raj, S. S., Sharma, A., Darbyshire, E., Reyes-Villegas, E., Allan, J.,
758 Chen, Y., Wang, X., Song, S., Pöhlker, M. L., Shi, L., Wang, Y., Kommula, S. M., Liu, T., Ravikrishna, R., McFiggans, G., Mickley, L. J., Martin, S. T., Pöschl, U., Andreae, M. O., and Coe, H.: Enhanced
760 aerosol particle growth sustained by high continental chlorine emission in India, Nat. Geosci. 2021 142, 14, 77–84, https://doi.org/10.1038/s41561-020-00677-x, 2021.

762 Holden, P. A., Gardea-Torresdey, J. L., Klaessig, F., Turco, R. F., Mortimer, M., Hund-Rinke, K., Cohen Hubal, E. A., Avery, D., Barceló, D., Behra, R., Cohen, Y., Deydier-Stephan, L., Ferguson, P.
764 L., Fernandes, T. F., Herr Harthorn, B., Henderson, W. M., Hoke, R. A., Hristozov, D., Johnston, J. M., Kane, A. B., Kapustka, L., Keller, A. A., Lenihan, H. S., Lovell, W., Murphy, C. J., Nisbet, R. M.,
766 Petersen, E. J., Salinas, E. R., Scheringer, M., Sharma, M., Speed, D. E., Sultan, Y., Westerhoff, P., White, J. C., Wiesner, M. R., Wong, E. M., Xing, B., Steele Horan, M., Godwin, H. A., and Nel, A. E.:
768 Considerations of Environmentally Relevant Test Conditions for Improved Evaluation of Ecological Hazards of Engineered Nanomaterials, Environ. Sci. Technol., 50, 6124–6145,
770 https://doi.org/10.1021/ACS.EST.6B00608/ASSET/IMAGES/LARGE/ES-2016-00608U_0003.JPEG, 2016.

772 Huang, W., Cao, J., Tao, Y., Dai, L., Lu, S. E., Hou, B., Wang, Z., and Zhu, T.: Seasonal Variation of Chemical Species Associated With Short-Term Mortality Effects of PM2.5 in Xi'an, a Central City in
774 China, Am. J. Epidemiol., 175, 556–566, https://doi.org/10.1093/AJE/KWR342, 2012.

IQAir: World air quality report 2021, Paper Knowledge . Toward a Media History of Documents, 43
776 pp., 2022.

Jain, S., Sharma, S. K., Choudhary, N., Masiwal, R., Saxena, M., Sharma, A., Mandal, T. K., Gupta,
778 A., Gupta, N. C., and Sharma, C.: Chemical characteristics and source apportionment of PM2.5 using PCA/APCS, UNMIX, and PMF at an urban site of Delhi, India, Environ. Sci. Pollut. Res., 24, 14637–
780 14656, https://doi.org/10.1007/S11356-017-8925-5/FIGURES/6, 2017.

Jain, S., Sharma, S. K., Vijayan, N., and Mandal, T. K.: Seasonal characteristics of aerosols (PM2.5 and

https://doi.org/10.5194/egusphere-2024-1385
Preprint. Discussion started: 12 July 2024

782 PM10) and their source apportionment using PMF: A four year study over Delhi, India, Environ. Pollut., 262, 114337, https://doi.org/10.1016/J.ENVPOL.2020.114337, 2020.

784 Jain, V., Tripathi, N., Tripathi, S. N., Gupta, M., Sahu, L. K., Murari, V., Gaddamidi, S., Shukla, A. K., and Prevot, A. S. H.: Real-time measurements of non-methane volatile organic compounds in the 786 central Indo-Gangetic basin, Lucknow, India: source characterisation and their role in O 3 and secondary organic aerosol formation , Atmos. Chem. Phys., 23, 3383–3408, 788 https://doi.org/10.5194/ACP-23-3383-2023, 2023.

Jat, R., Gurjar, B. R., and Lowe, D.: Regional pollution loading in winter months over India using high 790 resolution WRF-Chem simulation, Atmos. Res., 249, 105326, https://doi.org/10.1016/J.ATMOSRES.2020.105326, 2021.

792 Kastury, F., Smith, E., and Juhasz, A. L.: A critical review of approaches and limitations of inhalation bioavailability and bioaccessibility of metal(loid)s from ambient particulate matter or dust, Sci. Total 794 Environ., 574, 1054–1074, https://doi.org/10.1016/J.SCITOTENV.2016.09.056, 2017.

Kloog, I., Ridgway, B., Koutrakis, P., Coull, B. A., and Schwartz, J. D.: Long- and short-term exposure 796 to PM2.5 and mortality: Using novel exposure models, Epidemiology, 24, 555–561, https://doi.org/10.1097/EDE.0B013E318294BEAA, 2013.

798 Kumar, R. R., Soni, V. K., and Jain, M. K.: Evaluation of spatial and temporal heterogeneity of black carbon aerosol mass concentration over India using three year measurements from IMD BC observation 800 network, Sci. Total Environ., 723, 138060, https://doi.org/10.1016/J.SCITOTENV.2020.138060, 2020.

Lalchandani, V., Srivastava, D., Dave, J., Mishra, S., Tripathi, N., Shukla, A. K., Sahu, R., Thamban, 802 N. M., Gaddamidi, S., Dixit, K., Ganguly, D., Tiwari, S., Srivastava, A. K., Sahu, L., Rastogi, N., Gargava, P., and Tripathi, S. N.: Effect of Biomass Burning on PM2.5 Composition and Secondary 804 Aerosol Formation During Post-Monsoon and Winter Haze Episodes in Delhi, J. Geophys. Res. Atmos., 127, e2021JD035232, https://doi.org/10.1029/2021JD035232, 2022.

806 Lan, R., Eastham, S. D., Liu, T., Norford, L. K., and Barrett, S. R. H.: Air quality impacts of crop residue burning in India and mitigation alternatives, Nat. Commun. 2022 131, 13, 1–13, 808 https://doi.org/10.1038/s41467-022-34093-z, 2022.

Mahapatra, P. S., Sinha, P. R., Boopathy, R., Das, T., Mohanty, S., Sahu, S. C., and Gurjar, B. R.:

https://doi.org/10.5194/egusphere-2024-1385
Preprint. Discussion started: 12 July 2024

Seasonal progression of atmospheric particulate matter over an urban coastal region in peninsular India: Role of local meteorology and long-range transport, Atmos. Res., 199, 145–158, https://doi.org/10.1016/J.ATMOSRES.2017.09.001, 2018.

Majumdar, D., Mondal, R., Periyasamy, A., Barman, N., Dey, S., Roy, S., Mandal, P., Rao, P. S., and Sarkar, U.: Characterization and sources of fine carbonaceous aerosol in winter over a megacity on Indo-Gangetic plain, Urban Clim., 39, 100964, https://doi.org/10.1016/J.UCLIM.2021.100964, 2021.

Manchanda, C., Kumar, M., Singh, V., Hazarika, N., Faisal, M., Lalchandani, V., Shukla, A., Dave, J., Rastogi, N., and Tripathi, S. N.: Chemical speciation and source apportionment of ambient PM2.5 in New Delhi before, during, and after the Diwali fireworks, Atmos. Pollut. Res., 13, 101428, https://doi.org/10.1016/J.APR.2022.101428, 2022.

Mishra, S., Tripathi, S. N., Kanawade, V. P., Haslett, S. L., Dada, L., Ciarelli, G., Kumar, V., Singh, A., Bhattu, D., Rastogi, N., Daellenbach, K. R., Ganguly, D., Gargava, P., Slowik, J. G., Kulmala, M., Mohr, C., El-Haddad, I., and Prevot, A. S. H.: Rapid night-time nanoparticle growth in Delhi driven by biomass-burning emissions, Nat. Geosci. 2023 163, 16, 224–230, https://doi.org/10.1038/s41561-023-01138-x, 2023.

Mitra, S., Chakraborty, A. J., Tareq, A. M., Emran, T. Bin, Nainu, F., Khusro, A., Idris, A. M., Khandaker, M. U., Osman, H., Alhumaydhi, F. A., and Simal-Gandara, J.: Impact of heavy metals on the environment and human health: Novel therapeutic insights to counter the toxicity, J. King Saud Univ. - Sci., 34, 101865, https://doi.org/10.1016/J.JKSUS.2022.101865, 2022.

Nagar, P. K., Singh, D., Sharma, M., Kumar, A., Aneja, V. P., George, M. P., Agarwal, N., and Shukla, S. P.: Characterization of PM2.5 in Delhi: role and impact of secondary aerosol, burning of biomass, and municipal solid waste and crustal matter, Environ. Sci. Pollut. Res., 24, 25179–25189, https://doi.org/10.1007/s11356-017-0171-3, 2017.

Nalbandian, H.: Trace element emissions from coal, 89 pp., 2012.

Ojha, N., Sharma, A., Kumar, M., Girach, I., Ansari, T. U., Sharma, S. K., Singh, N., Pozzer, A., and Gunthe, S. S.: On the widespread enhancement in fine particulate matter across the Indo-Gangetic Plain towards winter, Sci. Reports 2020 101, 10, 1–9, https://doi.org/10.1038/s41598-020-62710-8, 2020.

Al osman, M., Yang, F., and Massey, I. Y.: Exposure routes and health effects of heavy metals on

https://doi.org/10.5194/egusphere-2024-1385
Preprint. Discussion started: 12 July 2024

children, BioMetals, 32, 563–573, https://doi.org/10.1007/S10534-019-00193-5/METRICS, 2019.

Paatero, P. and Hopke, P. K.: Rotational tools for factor analytic models, J. Chemom., 23, 91–100, https://doi.org/10.1002/cem.1197, 2009.

Pandey, A., Brauer, M., Cropper, M. L., Balakrishnan, K., Mathur, P., Dey, S., Turkgulu, B., Kumar, G. A., Khare, M., Beig, G., Gupta, T., Krishnankutty, R. P., Causey, K., Cohen, A. J., Bhargava, S., Aggarwal, A. N., Agrawal, A., Awasthi, S., Bennitt, F., Bhagwat, S., Bhanumati, P., Burkart, K., Chakma, J. K., Chiles, T. C., Chowdhury, S., Christopher, D. J., Dey, S., Fisher, S., Fraumeni, B., Fuller, R., Ghoshal, A. G., Golechha, M. J., Gupta, P. C., Gupta, R., Gupta, R., Gupta, S., Guttikunda, S., Hanrahan, D., Harikrishnan, S., Jeemon, P., Joshi, T. K., Kant, R., Kant, S., Kaur, T., Koul, P. A., Kumar, P., Kumar, R., Larson, S. L., Lodha, R., Madhipatla, K. K., Mahesh, P. A., Malhotra, R., Managi, S., Martin, K., Mathai, M., Mathew, J. L., Mehrotra, R., Mohan, B. V. M., Mohan, V., Mukhopadhyay, S., Mutreja, P., Naik, N., Nair, S., Pandian, J. D., Pant, P., Perianayagam, A., Prabhakaran, D., Prabhakaran, P., Rath, G. K., Ravi, S., Roy, A., Sabde, Y. D., Salvi, S., Sambandam, S., Sharma, B., Sharma, M., Sharma, S., Sharma, R. S., Shrivastava, A., Singh, S., Singh, V., Smith, R., Stanaway, J. D., Taghian, G., Tandon, N., Thakur, J. S., Thomas, N. J., Toteja, G. S., Varghese, C. M., Venkataraman, C., Venugopal, K. N., Walker, K. D., Watson, A. Y., Wozniak, S., Xavier, D., Yadama, G. N., Yadav, G., Shukla, D. K., Bekedam, H. J., et al.: Health and economic impact of air pollution in the states of India: the Global Burden of Disease Study 2019, Lancet Planet. Heal., 5, e25–e38, https://doi.org/10.1016/S2542-5196(20)30298-9, 2021.

Pandey, P. and Soni., D.: ENRICHMENT OF HEAVY METAL IN AMBIENT AIR OF LUCKNOW CITY AND ITS POTENTIAL HEALTH HAZARDS., Int. J. Adv. Res., 5, 299–309, https://doi.org/10.21474/IJAR01/5533, 2017.

Pant, P., Shukla, A., Kohl, S. D., Chow, J. C., Watson, J. G., and Harrison, R. M.: Characterization of ambient PM2.5 at a pollution hotspot in New Delhi, India and inference of sources, Atmos. Environ., 109, 178–189, https://doi.org/10.1016/j.atmosenv.2015.02.074, 2015.

Rai, P., Chakraborty, A., Mandariya, A. K., and Gupta, T.: Composition and source apportionment of PM1 at urban site Kanpur in India using PMF coupled with CBPF, Atmos. Res., 178–179, 506–520, https://doi.org/10.1016/J.ATMOSRES.2016.04.015, 2016.

https://doi.org/10.5194/egusphere-2024-1385
Preprint. Discussion started: 12 July 2024

Rai, P., Furger, M., El Haddad, I., Kumar, V., Wang, L., Singh, A., Dixit, K., Bhattu, D., Petit, J. E., Ganguly, D., Rastogi, N., Baltensperger, U., Tripathi, S. N., Slowik, J. G., and Prévôt, A. S. H.: Real-time measurement and source apportionment of elements in Delhi's atmosphere, Sci. Total Environ., 742, 140332, https://doi.org/10.1016/J.SCITOTENV.2020.140332, 2020.

Rehman, K., Fatima, F., Waheed, I., and Akash, M. S. H.: Prevalence of exposure of heavy metals and their impact on health consequences, J. Cell. Biochem., 119, 157–184, https://doi.org/10.1002/JCB.26234, 2018.

Reyes, J. W.: LEAD EXPOSURE AND BEHAVIOR: EFFECTS ON ANTISOCIAL AND RISKY BEHAVIOR AMONG CHILDREN AND ADOLESCENTS, Econ. Inq., 53, 1580–1605, https://doi.org/10.1111/ECIN.12202, 2015.

Sanders, T., Liu, Y., Buchner, V., and Tchounwou, P. B.: Neurotoxic effects and biomarkers of lead exposure: A review, Rev. Environ. Health, 24, 15–45, https://doi.org/10.1515/REVEH.2009.24.1.15/MACHINEREADABLECITATION/RIS, 2009.

Sharma, S. K. and Mandal, T. K.: Chemical composition of fine mode particulate matter (PM2.5) in an urban area of Delhi, India and its source apportionment, Urban Clim., 21, 106–122, https://doi.org/10.1016/j.uclim.2017.05.009, 2017.

Sharma, S. K., Sharma, A., Saxena, M., Choudhary, N., Masiwal, R., Mandal, T. K., and Sharma, C.: Chemical characterization and source apportionment of aerosol at an urban area of Central Delhi, India, Atmos. Pollut. Res., 7, 110–121, https://doi.org/10.1016/j.apr.2015.08.002, 2016.

Shukla, A. K., Lalchandani, V., Bhattu, D., Dave, J. S., Rai, P., Thamban, N. M., Mishra, S., Gaddamidi, S., Tripathi, N., Vats, P., Rastogi, N., Sahu, L., Ganguly, D., Kumar, M., Singh, V., Gargava, P., and Tripathi, S. N.: Real-time quantification and source apportionment of fine particulate matter including organics and elements in Delhi during summertime, Atmos. Environ., 261, 118598, https://doi.org/10.1016/J.ATMOSENV.2021.118598, 2021.

Shukla, A. K., Tripathi, S. N., Canonaco, F., Lalchandani, V., Sahu, R., Srivastava, D., Dave, J., Thamban, N. M., Gaddamidi, S., Sahu, L., Kumar, M., Singh, V., and Rastogi, N.: Spatio-temporal variation of C-PM2.5 (composition based PM2.5) sources using PMF*PMF (double-PMF) and single-combined PMF technique on real-time non-refractory, BC and elemental measurements during post-

https://doi.org/10.5194/egusphere-2024-1385
Preprint. Discussion started: 12 July 2024

894 monsoon and winter at two sites in Delhi, India, Atmos. Environ., 293, 119456, https://doi.org/10.1016/J.ATMOSENV.2022.119456, 2023.

896 Shukla, A.K., Tripathi, S.N., Talukdar, S., Murari, V., Gaddamidi, S., Manousakas, M. I., Lalchandani, V., Dixit, K., Ruge, V. M., Khare, P., Kumar, M., Singh, V., Rastogi, N., Tiwari, S., Srivastava, A. K.,

898 Ganguly, D., Dallenbach K. R., and Prevot, A. S. H. Sources and meteorology influencing highly-time resolved PM2.5 trace elements at 3 urban sites in extremely polluted Indo Gangetic Plain in India,

900 Measurement_Report_Data_21-06-2024, https://doi.org/10.5281/zenodo.12212768, 2024

Stefenelli, G., Pospisilova, V., Lopez-Hilfiker, F. D., Daellenbach, K. R., Hüglin, C., Tong, Y.,

902 Baltensperger, U., Prévôt, A. S. H., and Slowik, J. G.: Organic aerosol source apportionment in Zurich using an extractive electrospray ionization time-of-flight mass spectrometer (EESI-TOF-MS) – Part 1:

904 Biogenic influences and day–night chemistry in summer, Atmos. Chem. Phys., 19, 14825–14848, https://doi.org/10.5194/acp-19-14825-2019, 2019.

906 Strickland, M. J., Hao, H., Hu, X., Chang, H. H., Darrow, L. A., and Liu, Y.: Pediatric Emergency Visits and Short-Term Changes in PM2.5 Concentrations in the U.S. State of Georgia, Environ. Health

908 Perspect., 124, 690–696, https://doi.org/10.1289/EHP.1509856, 2015.

Tchounwou, P. B., Yedjou, C. G., Patlolla, A. K., and Sutton, D. J.: Heavy metal toxicity and the

910 environment, EXS, 101, 133–164, https://doi.org/10.1007/978-3-7643-8340-4_6/COVER, 2012.

Tobler, A., Bhattu, D., Canonaco, F., Lalchandani, V., Shukla, A., Thamban, N. M., Mishra, S.,

912 Srivastava, A. K., Bisht, D. S., Tiwari, S., Singh, S., Močnik, G., Baltensperger, U., Tripathi, S. N., Slowik, J. G., and Prévôt, A. S. H.: Chemical characterization of PM2.5 and source apportionment of

914 organic aerosol in New Delhi, India, Sci. Total Environ., 745, 140924, https://doi.org/10.1016/j.scitotenv.2020.140924, 2020.

916 Tremper, A. H., Font, A., Priestman, M., Hamad, S. H., Chung, T. C., Pribadi, A., Brown, R. J. C., Goddard, S. L., Grassineau, N., Petterson, K., Kelly, F. J., and Green, D. C.: Field and laboratory

918 evaluation of a high time resolution x-ray fluorescence instrument for determining the elemental composition of ambient aerosols, Atmos. Meas. Tech., 11, 3541–3557, https://doi.org/10.5194/amt-11-

920 3541-2018, 2018.

Wani, A. L., Ara, A., and Usmani, J. A.: Lead toxicity: a review, Interdiscip. Toxicol., 8, 55,

https://doi.org/10.5194/egusphere-2024-1385
Preprint. Discussion started: 12 July 2024

https://doi.org/10.1515/INTOX-2015-0009, 2015.

Yadav, S., Tripathi, S. N., and Rupakheti, M.: Current status of source apportionment of ambient aerosols in India, Atmos. Environ., 274, 118987, https://doi.org/10.1016/J.ATMOSENV.2022.118987, 2022.

Zavala, M., Molina, L. T., Maiz, P., Monsivais, I., Chow, J. C., Watson, J. G., Munguia, J. L., Cardenas, B., Fortner, E. C., Herndon, S. C., Roscioli, J. R., Kolb, C. E., and Knighton, W. B.: Black carbon, organic carbon, and co-pollutant emissions and energy efficiency from artisanal brick production in Mexico, Atmos. Chem. Phys., 18, 6023–6037, https://doi.org/10.5194/ACP-18-6023-2018, 2018.